Dielectrophoresis to Analyze Mouse Hepatitis Coronavirus Particles

by

Matthew McFadden

A Thesis Presented in Partial Fulfillment
of the Requirements for the Degree
Master of Science

Approved November 2023 by the
Graduate Supervisory Committee:

Brenda G. Hogue, Co-Chair
Mark Hayes, Co-Chair
Jennifer Blain Christen
Shaopeng Wang

ARIZONA STATE UNIVERSITY

December 2023

ABSTRACT

Detection technologies and physical methods used for separation of complex molecules can be effective tools in research when applied to bioparticles including, but not limited to, bacteria, viruses, and proteins. Dielectrophoresis (DEP) is a technique that has been used in microfluidics for separation and concentration of bioparticles, with the benefits of not requiring custom primers, utilizing small sample sizes, and relatively quick separation times for rapid identification of pathogens such as viruses. As demonstrated in this study, a DEP device using polydimethylsiloxane (PDMS) as an insulator was used for the identification and separation of a mouse hepatitis coronavirus (MHV), a model coronavirus that only infects mice. Results indicate that, using 10 microliters of MHV test sample diluted in buffer, the virus can be identified and separated within 30 seconds using DC voltage of 800 V.

DEDICATION

This thesis is dedicated to my family, friends and coworkers who have taken the time to show compassion and teach me the methods used in this thesis and many more.

ACKNOWLEDGMENTS

To the Hogue lab and the Mark Hayes research group who enabled me to work on my master's and have taken the time and resources that allowed me to grow.

TABLE OF CONTENTS

LIST OF FIGURES

Figure Page

LIST OF TABLES

CHAPTER 1

INTRODUCTION

New methods of bioparticle separation and detection have a wide range of applications from healthcare to scientific discovery. More sensitive detection systems that can distinguish even small numbers of genetic mutations are needed to detect different pathogen isoforms that may evade standard identification approaches for diagnosis and thus delay treatments and protection. In current virology, coronavirus variants arise that have caused reduced effectiveness of vaccines. Early identification of such mutations could allow healthcare systems to better respond at earlier times to severe infections. Developing new methods that distinguish virus mutants in real time could open avenues for the discovery of new viral pathogens or mutations of concern that could disrupt medical systems around the world. Early detection of new mutations would potentially improve early responses and allow earlier development of new vaccines and other treatments. Currently, the World Health Organization has tracked 11 variant families of SARS-CoV-2 not including additional variants of concern. [1]

Overview of methods of virus detection

From the beginning of public health and discovery of microbial pathogens, the original method of indicating a viral infection is made through observation of a host and associated signs and symptoms (rash, cough, fever, cellular death etc.). As technology and scientific progress has continued, modern methods of pathogen detection have drastically improved from when the scientific community first identified viruses in 1898 with the Tobacco Mosaic Virus. [4] The current methods of virus particle detection have varied in sensitivity and use over time. The original gold standard for biological detection of viruses is the plaque assay, due to its sensitivity and accuracy to detect intact infectious viral particles from its inception in the 1950s and 1960's. [6] This test used an overlay of virus-sensitive cells that can be infected by virus for identification of the plaque forming unit (pfu). Plaque assay, while still a useful tool, is not without its drawbacks: the test requires specific cell lines for different viruses, and is also time consuming, and labor intensive.

The plaque assay also does not register inactivated viruses, nor does it measure the total number of virus particles in a test sample.

Polymerase chain reaction (PCR), the detection of virus nucleic acids via the amplification of the viral genomic sequence, is the current gold standard method for precise detection of viruses. This technology has improved to now include Real Time Quantitative Polymerase Chain Reaction allowing precise quantification of genome copy numbers. There are limitations with this method, as it requires specific primers that need to be synthesized to identify the specific viral genome that is being detected, along with requiring specially equipped laboratory facilities and trained users to operate. [7]

Viral antigen detection (VAD) shares many similarities with original methods of detecting viruses as it requires a host immune response to enable the detection technology. VAD is one of the most successful and diverse strategies including, but not limited to, Western blotting, enzyme linked immunosorbent assay (ELISA), and antigen lateral flow assays. The use of this VAD technology has proliferated into use in the public as different methods have seen significant decreases in cost-per-assay and ease of usage. Additionally, the use of VAD by the public has seen major expansion due to the COVID-19 pandemic. [10] VAD is a more generic assay but can be adapted to identify specific genetic changes in infectious viruses due to antigen changes with different virus mutations that can require changes to the test to account for progressive acquisition of mutations. [8] VAD however often suffers from limited concentration detection and reduced sensitivity.

Electron Microscopy (EM) was first used to visualize a virus, originally by examining a strain of Tobacco Mosaic Virus. [10] EM has been long used in virology to study virus particles as major steps to understanding virus biology and educating the public about what viruses physically look like. In virology research, this technology has progressed into multiple forms from transmission electron microscopy (TEM) and cryo electron microscopy, the latter used for accurate information about structural details of viruses. The current exploitation of EM for viral

examination requires samples first to be fixed by negative staining, a process that utilizes hazardous chemicals. This EM staining process, while useful for research and identification of novel pathogens, has limitations that include prohibitive cost for the electron microscope, hazardous materials, limited only to well-equipped laboratories, and nonspecific sensitivity due to detecting topography.

Dynamic Light Scattering (DLS), while not originally developed for virus detection, has been used as a method of virion detection and determining concentrations of many classes of small particles in solution. DLS primarily works by light scattering of samples suspended in solution as a method of detection using Brownian motion to calculate the physical sizes of the particles. Current DLS systems often use laser light as a method of illuminating particles using Rayleigh Scattering allowing the detection of particles including even the smallest virions. The strengths of this detection method include the non-specificity of this system for detecting any defractable particles suspended in solution. A drawback of this method is that the system is expensive to run, nonspecific to virus isoforms, and requires trained personnel to use effectively. [11]

Overview of Mouse Hepatitis Virus

This thesis exploits mouse hepatitis virus (MHV), a mouse coronavirus, as a standard test virus. MHV is a level 2 biosafety RNA virus of the Coronaviridae family that has been commonly used as a safer control substitute for level 3 biosafety SARS-CoV-2, for humans, to better understand coronavirus infections and structure. In previous experiments, the virus was first isolated in 1949, [2] MHV is a polymorphic virus with an average size of 80 nm and infects only mice. The structure of the virus consists of district protein entities, the spike protein (S), membrane protein (M), envelope protein (E), nucleocapsid (N) and the RNA viral genome.

Overview of PENN98

In addition to MHV-A59 a mutant virus PENN98 was procured from Susan Weiss, University of Pennsylvania. This virus shares much of the same genome as MHV-A59 with 2 main modifications, as seen in Figure 1. The spike protein gene is replaced with one that is found on MHV-2, and ORF 4 coding region is replaced with a GFP gene. GFP is expressed during replication of the virus but is not incorporated into viral particles.

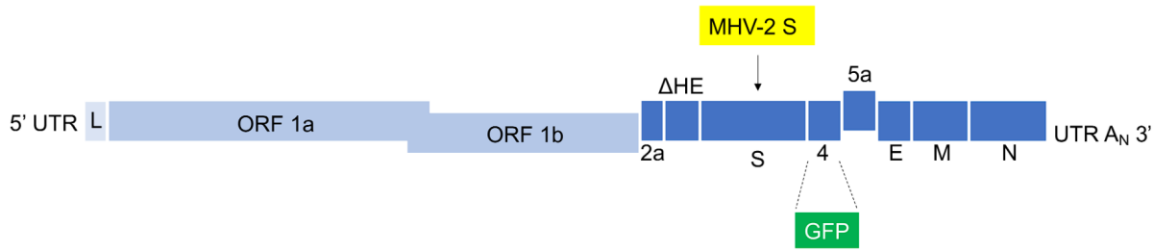

Figure 1. Representation of MHV A59 and PENN98 genome with a green GFP box highlighting the area GFP found in genome of PENN98, with Spike protein found from MHV-2 in PENN98.

Overview of Sindbis Virus

This thesis also exploits Sindbis, an RNA virus and human pathogen, as an additional test virus for comparison with MHV-A59. Sindbis is a Level 2 Biosafety (BSL2) RNA virus of the Togaviridae family in the Alphavirus genus and is used to better understand Alphavirus infections and structure. Sindbis virus is transmitted by mosquitoes and causes clinical disease in Northern Europe (Finland etc.). Sindbis is genetically unrelated to MHV and its virion structure is distinct from those of coronaviruses in terms of protein composition and charge, but It's size (70 nm) is close to that of MHV-A59 (80-100 nm). Sindbis virus was first isolated in 1952 north of Cairo and has been used extensively in research laboratories as a model togavirus. [22] Sindbis virus particles have an average size of 70 nm, possess an 11.7kb genome, and as a typical arbovirus, transmits via mosquitoes. The structure of the virus particle is composed of distinct components: capsid, E1 trimer, E2 trimer, envelope, and the RNA viral genome.

Along with using Sindbis virus heat resistant (SVHR), this thesis overviews the purification of two other viruses, Sindbis virus Venus (SVV) with a Venus tag incorporated into the structure of the virus that can fluoresce green, and a Sindbis virus Venus tetracysteine (SVVT) identical to SVV except with an additional tetracysteine attached to the capsid of the virus.

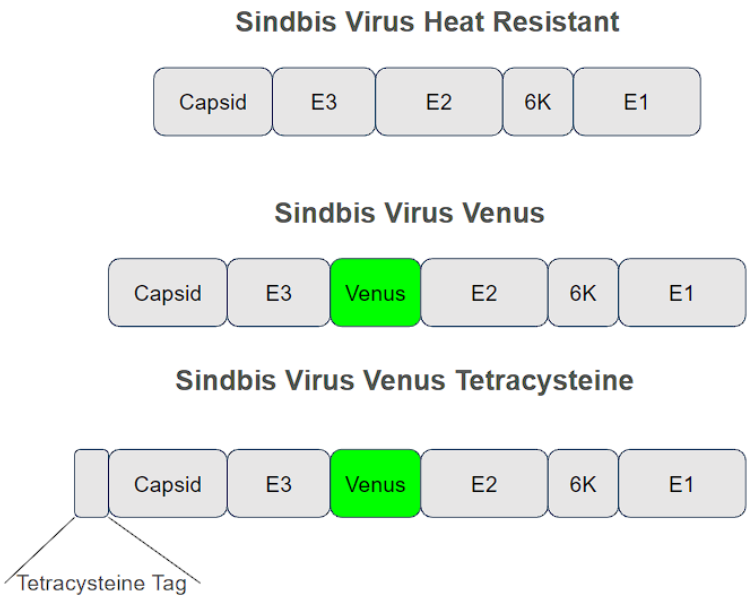

Figure 2. A simple diagram showing the differences between the changes between Sindbis virus heat resistant, Sindbis virus Venus and Sindbis virus Venus tetracysteine. Tetracysteine Tag has the following sequence, “TGCTGCCCCGGCTGCTGC”.

Overview of Laser Light Scattering

Lasers have been commercially available since 1960, based on groundbreaking studies by Maiman, and as the technology has matured it has been used for a multitude of scientific experiments, ranging from spectroscopy to laser-included fluorescence microscopy. [21] This thesis primarily focuses on using laser light of various colors as a method of illumination of virus particles that are generally below the detection range of bright field microscopes, and as a method of characterizing particles of various types in solution. By using Brownian motion to assess the size of particles and count the number of particles, the method is versatile in

assessing the size and number of refracting particles in solution that are unlabeled. Following Figure 3 demonstrates a basic diagram of laser light scattering off a particle-containing sample in solution.

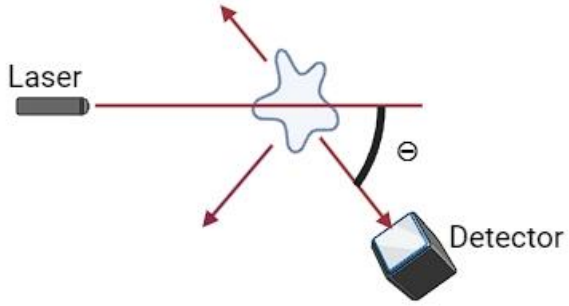

Figure 3. Showing laser light scattering off a sample into a detector for idealized light scattering.

$$I = I_0 \frac{1 + \cos^2\theta}{2R^2} \left(\frac{2\pi}{\lambda}\right)^4 \left(\frac{n^2 - 1}{n^2 + 2}\right)^2 r^6$$

The intensity of laser light scattering can be described by the previous idealized equation, where *I* is the intensity of the laser light reaching the detector, Θ is the angle between the laser and the detector, λ is the wavelength of the laser, *n* is the index of refraction of the sample, *r* is the radius of the particle, *R* is the distance to the detector. This equation can be used for the description of laser light scattering including Tyndal effect, light scattering from particles larger than the wavelength of light, and Rayleigh light scattering from particles smaller than the wavelength of light. Rayleigh scattering is possible due to the laser light scattering off the change of refractive index between the particles and the surrounding medium, giving a larger target that the laser light can reflect off. In this work, the relative abilities of laser light of various colors and

intensities was compared in order to assess the optimal illumination conditions for the various viruses tested.

Overview of Dielectrophoresis

Dielectrophoresis (DEP) utilizes a non-uniform electric field that interacts with a particle suspended in a solution. The particle is subjected to a DEP effect even when the particle does not have a charge. Each particle is affected to varying degrees depending on the analyte's size, shape, polarizability, heterogeneity, charge, internal, and external structure. DEP was first described in the 1950's by Herbert Pohl. [12]

$$F = 2\pi r^3 \varepsilon_m \dot{R}e(f_{CM})\nabla E^2$$

Dielectrophoresis force can be described with the previous equation where *r* represents the radius of the particle, ε_m is the permittivity of the medium, f_{cm} Clausius-Mossotti factor, ∇E is the gradient in the electrical field. Though this equation and description best fits how the forces work for particles that are above 1000 nm in size, the equation does not match the observed phenomenon for particles smaller than 1000 nm. To date, there is recorded published research demonstrating DEP analysis of Sindbis virus particles that are about 70nm in diameter. [3]

The method of using progressively changing geometry to detect distinct areas within a microfluidic device was first described in 2007. [14] This method has the benefits of being able to interrogate particles using different gradients in the electrical field. The expression of electrokinetic and dielectrophoretic capture can be described with mathematical expression shown in equation (3) below:

$$\frac{\Delta|E|^2 \cdot E}{E^2} \geq \frac{\mu_{EK}}{\mu_{DEP}}$$

where $\mu_{EK}$is electroosmosis mobility and electrophoresis mobility, μ_{DEP} is dielectrophoresis and *E* is the electrical field. With this understanding, the equation gives a better picture but is still limited

about the different factors such as electroosmosis and electrophoresis can play in determining the forces on bioparticles such as virions within a DEP device. [13]

Figure 4. Schematic showing the top view showing the microfluidic apparatus used in insulator based DEP. The device is roughly 4 cm in length with 24 teeth like structures constructed of PDMS with the largest teeth gap being 30um and the smallest being 3um.

The progressively decreasing gaps on the insulated teeth within the device continue to increase the electrical field gradient with every decrease in the gap as demonstrated in Figure 5.

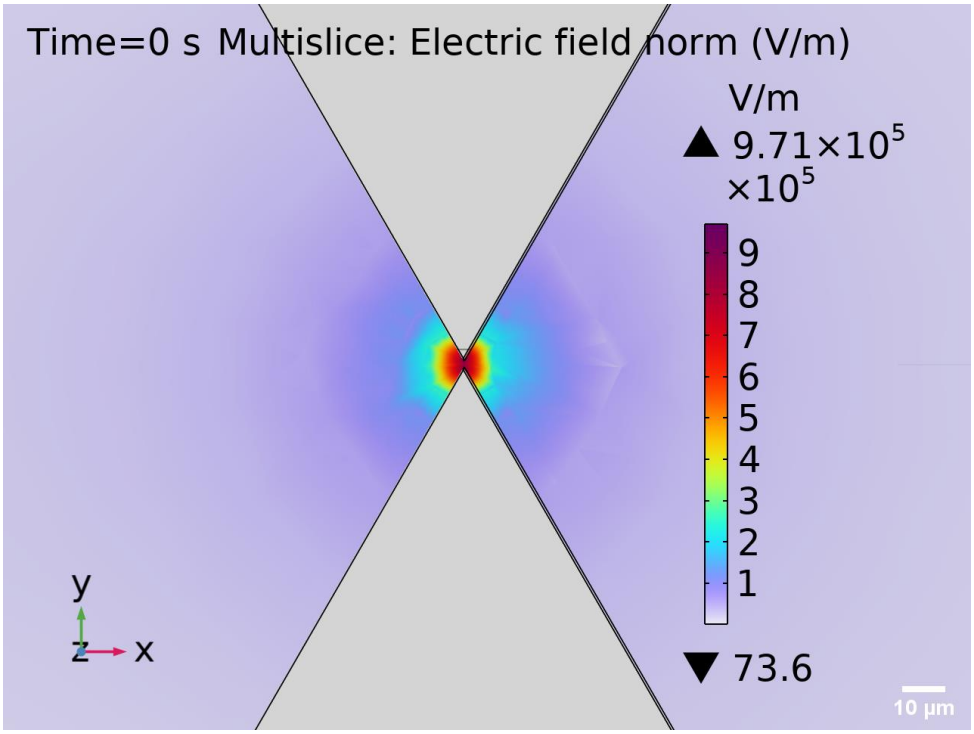

Figure 5. 3D COMSOL simulation of the electrical field gradient via the PDMS microfluidic device. Visualizing the zoomed in electrical field gradient near the teeth of the device with red indicating location of highest gradient change and purple being uniform electrical field gradient induced by 1000V applied though the device.

Previous research with bacteria [17], proteins [15-16], and viruses [3] using DEP shows that this technique can capture and separate bioparticles at under the 1000 nm diameter range originally thought to be impossible due to the current understanding of the Clausius-Mossotti factor in the original DEP equation. What has not been fully explored was the sensitivity of DEP to changes in this nanometer range of sizes of test particles.

CHAPTER 2

CUSTOM SCATTER SYSTEM DEVELOPMENTAL INSIGHTS

In the pursuit of advancing scientific instrumentation and our understanding of DEP technology, this thesis has sought to adapt and adjust laser light scattering DEP systems to specifically identify and characterize virus particles (virions). This thesis embarks on a journey through the developmental insights acquired over time with a focus on the transition from the commercially available system, the NS300, to the creation of the custom DEP scatter system, and a focus on methods of reducing the failure rate of microfluidic DEP devices. The NS300, while a commendable system, and used for the characterization of viral samples, is not designed with the needs of DEP optimization experiments in mind. While offering valuable insights, challenges have driven the development of more sophisticated and tailored solutions. This evolution represents a step forward in the quest to refine and enhance laser (light amplification by the stimulated emission of radiation) light scattering as a detection method useful for DEP experiments, ultimately contributing to a versatile tool for scientific research, characterization, and analysis of unlabeled viral samples and other bioparticles below the resolution limit of light microscopy. This thesis describes the challenges, innovations, acquired datasets, and benefits associated with this transition, shedding light on the developmental journey that has led to the current state of laser light scattering DEP technology and some thoughts on the next steps in development.

Initial NS300 Experimental Developmental Insights

The first testing of DEP devices on the NS300 can be seen in Figure 6 with the DEP device placed on top of the laser light module.

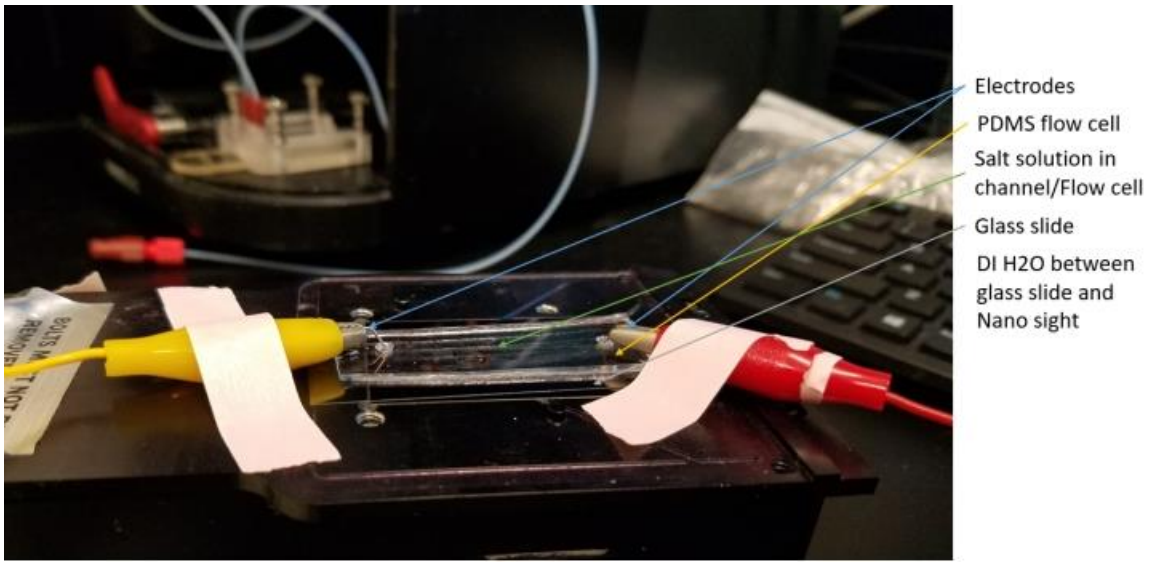

Figure 6 A photo and description of the first version of a microfluidic DEP device using 50 mw green laser 532nm laser light scattering as a method of illumination, with the electrodes connected to a power supply, and a glass slide sitting above the laser module with 50ul of water above the laser.

This initial method of testing using the commercial system provided insight into what changes would make the next generation of devices more effective. Not requiring a liquid layer between the laser and the DEP device leads to a simplification of testing because the liquid is not evaporating, avoiding the changing of solution mediums that the laser light must pass through and allowing for freer movement between the device and the laser module after the liquid has evaporated between the device runs. When the liquid had evaporated between the device runs, it would make the repositioning of the DEP device particularly difficult as it would stick to the surface of the NS300 and sometimes cause the glass slide with the PDMS to shatter from the force of movement.

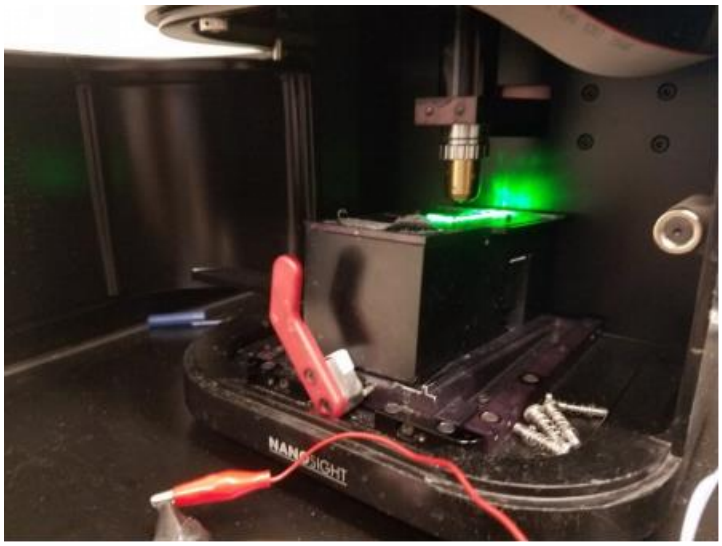

Figure 7. Photo of the microfluidic Integrated with a Nanosight NS300 for data gathering without the power supply connected.

An additional benefit of moving to a more open plan is that the connecting of the electrical wires to the microfluidic device and the movement of the DEP device would be easier when not being performed in a closed container with no easy side access, as seen in Figure 7. For data gathering, the method of retrieving data from the NS300 system was not ideal, due to a lack of access to the output of the camera system, a screen recording of the output of the camera was used, instead of the more data-dense direct output of the camera. This resulted in a low signal-to-noise ratio as seen in Figure 8. Additionally, experiments are not run to 2000 V or higher due to the discharges at the tips of the PDMS device, caused by the electric current passing through them.

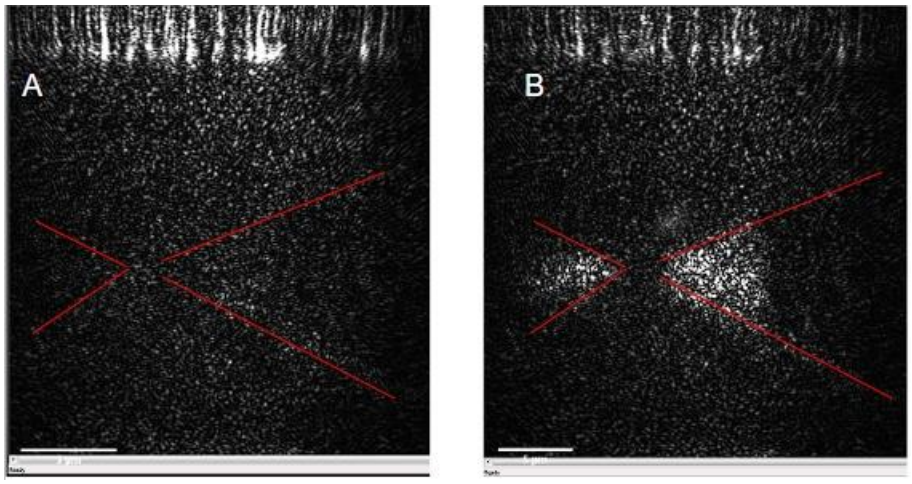

Figure 8. DEP data gathered on a NS300 during excitation with 2000V of DC power supplied to the device. The red lines show the edges of the PDMS teeth. Image A shows the 3 um gap gate before power 2000 V is supplied to the microfluidic device, Image B shows the device after 25 seconds of power being supplied.

Sindbis virus data was gathered using this initial system, as seen in Figure 9. As described above, the signal-to-noise ratio when using the original testing setup with the NS300 made definitive conclusions about the results unlikely. As testing was completed the device for this experiment had an obstruction of PDMS in another section of the device, making this dataset a null result, as the fluid flow through the device was interrupted. When precisely that happened during the experiment is unknown.

During this time, the COVID-19 pandemic began and SARS-CoV-2 became a primary focus of experimental results. A surrogate related coronavirus MHV-A59 became the primary viral focus point of the subsequent experiments that could be done at BSL 2 Level.

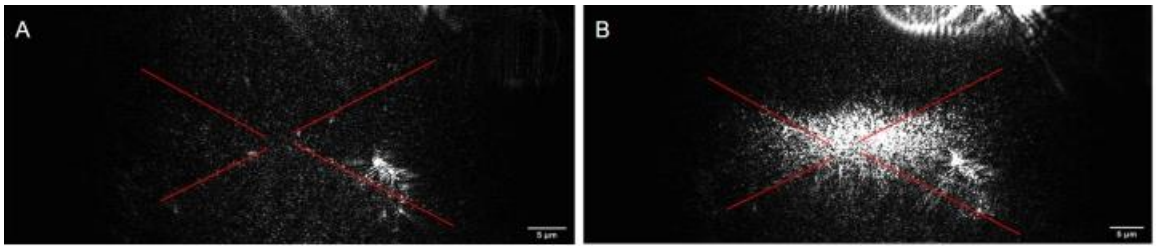

Figure 9. DEP data gathered on a NS300 with 1200V of DC power supplied to the device after being filled with $10^8(\frac{particles}{ml})$ of Sindbis. The red lines show the edges of the PDMS teeth. Image A shows the 3 um gap gate before power 1200 V is supplied to the microfluidic device, Image B shows the device after 20 seconds of power being supplied.

Initial LN10 Experimental Developmental Insights

NanoSight LN10 as seen in Figure 10. is an older edition of an NS300 and uses the same laser module but it is not enclosed in the same restrictive cover and allows the mounting of another camera that can directly record data. While this is an improvement over the NS300 experimental setup and allowed for a greater data-to-noise ratio due to getting data directly from the system for DEP experiments, there were a few drawbacks, primarily it was a light scattering artifact that looked like a barcode that could mask the collections of samples near the teeth of the gate.

As seen in Figure 11 below there is a marked improvement in the data gathered compared to Figure 9, as the wider frame of view and higher fidelity of data, allowed the gathering of preliminary data on MHV PENN98, but this data is in the developmental insights section and not results because during the post mortem in checking of the device, a clog was discovered.

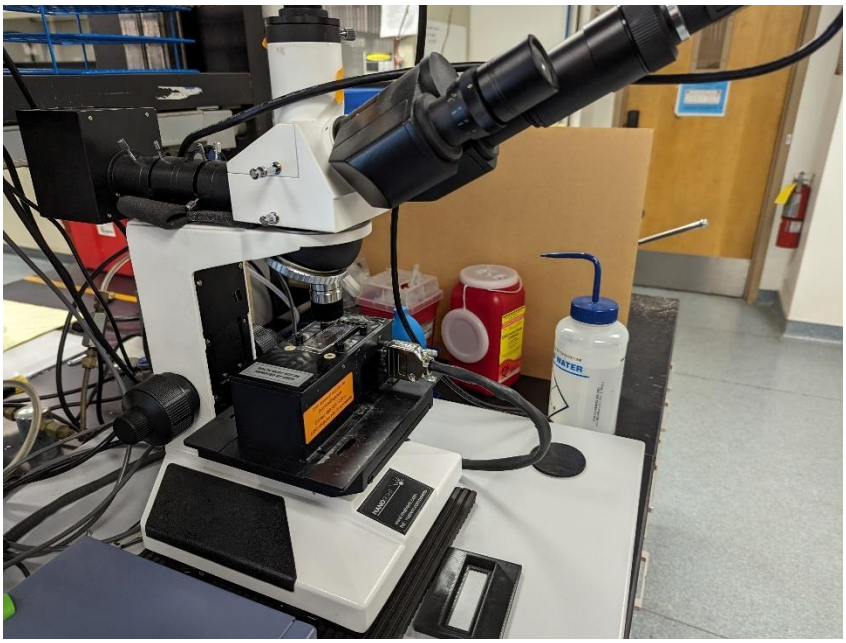

Figure 10. Image of the LN10 with a DEP device placed on top.

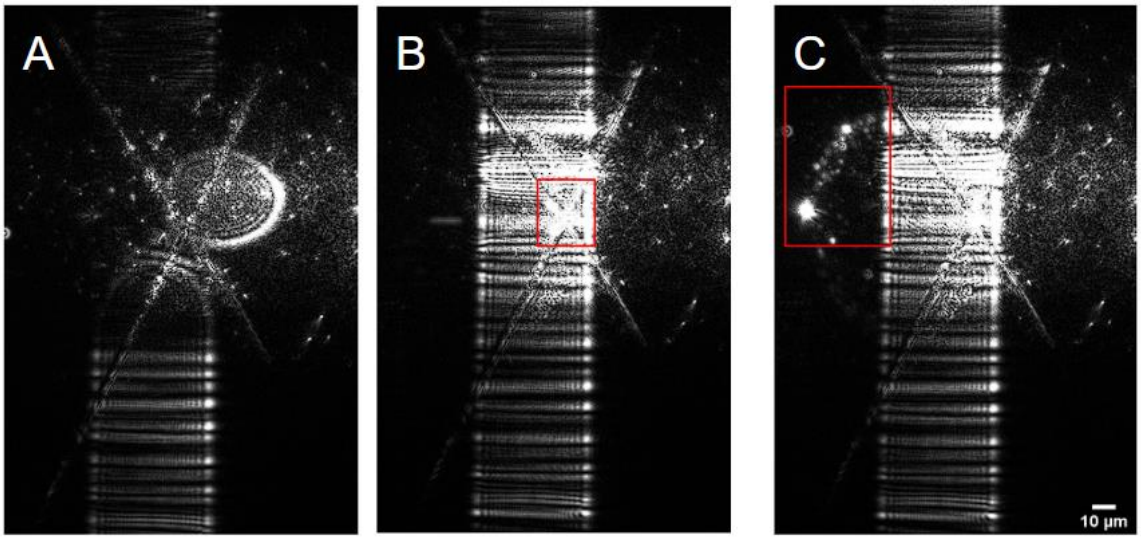

Figure 11. DEP experimental data was collected on the LN10, using MHV PENN98 as the test sample. (A) The before the voltage is turned on in the device. (B) It is after the DC 1500 V has been turned on for 20 seconds, the red box highlights where the PENN98 samples have been collected. (C) After 1500V has been turned off, the red box highlights the sample that had been collected near the gate and the sample released and is spreading back out.

Initial Custom Scatter System Experimental Developmental Insights

The Custom Scatter System (CSS) is described in the Figure 12 below along with Figure 13 that shows the experimental setup. The primary differences between the NS300 testing setup and the CSS is that the objective below the DEP device and the CSS utilizes three 100 mw red 663 nm lasers above the device. There are also the benefits of not requiring a liquid barrier to move the device and for the laser light path. Additionally, using a more optimally set up camera system, the data can be directly output from the camera, and no data was lost due to using screen recording to save data. This method increased the ratio of signal to noise allowing for higher resolution and information from DEP laser light experiments.

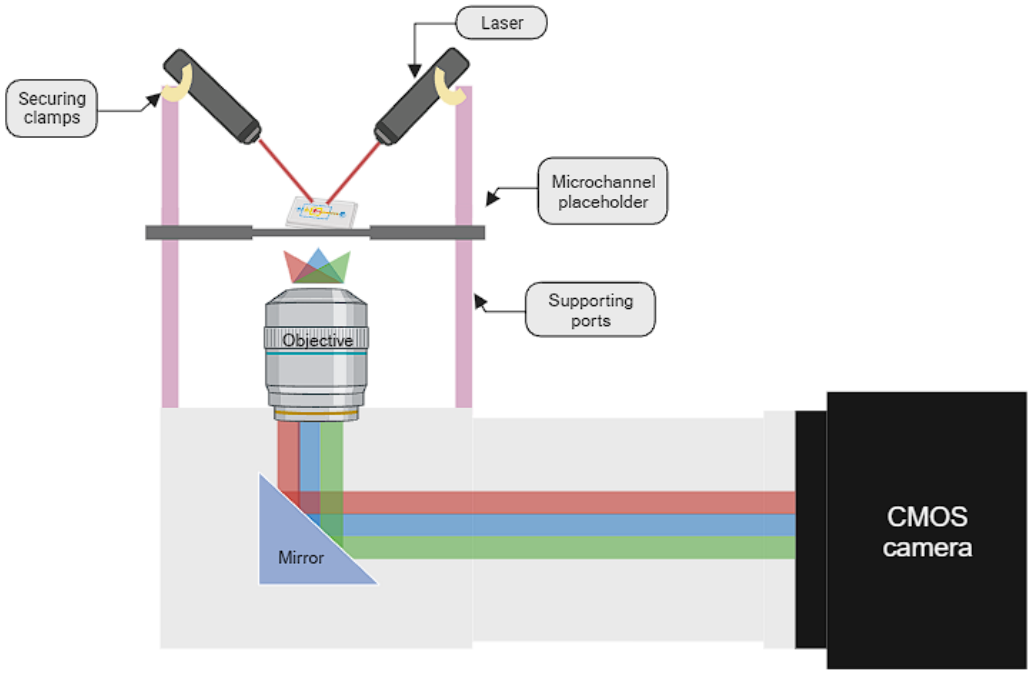

Figure 12 Schematic depicting the current custom scatter experimental setup with 3 Red lasers (663 nm) lasers used as an illumination of a DEP device and the light path that is taken to the camera. (Illustration modified from original created by Hoai Nguyen)

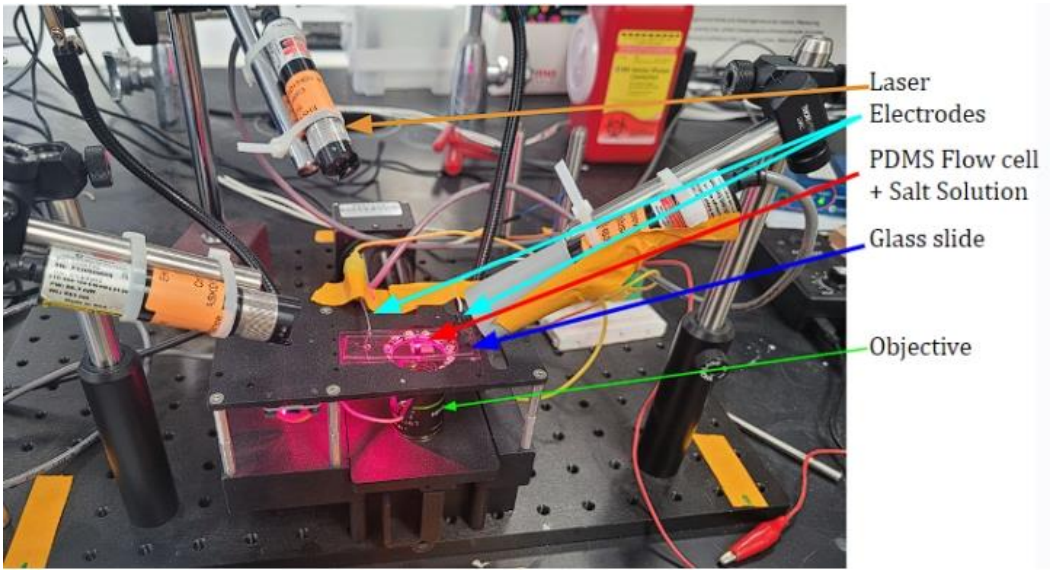

Figure 13. An image of the custom scatter experimental setup, showing 3 red 663 nm lasers used as methods of illumination, platinum electrodes inserted into the dep device, glass slide that the PDMS is resting on and the objective for the camera system.

The CSS is not a static device and continuous modifications and updates are constantly being performed on the device to improve its qualities. One advancement would be to use a lower power blue 450 nm laser instead of the current setup of three 663 nm lasers. As shown in Figure 14 is a qualitative comparison showing both sets of lasers illuminating the 50 nm particles around gate 1. The benefit of using a lower power laser is that it reduces the amount of laser heating of the samples in the DEP device. Additionally, smaller wavelengths of lasers have a greater chance of deflecting off smaller targets due to Rayleigh scattering.

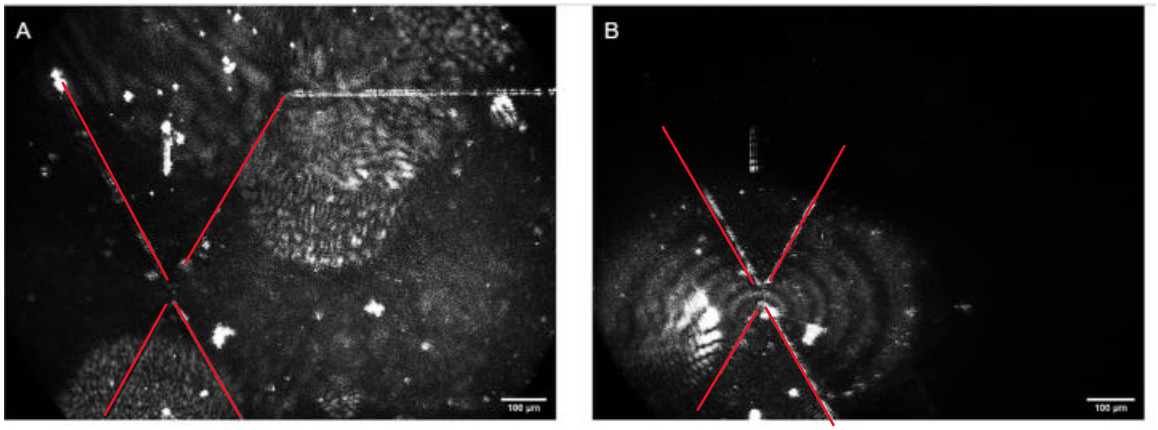

Figure 14. DEP device showing 2 types of illumination filled with $10^{10}(\frac{particles}{ml})$ of 50nm polystyrene beads. Image A is illuminated with three 100 mw red 663 nm lasers above the device. Image B is 1 blue 10 mw laser. Red lines added to show edges of DEP device's teeth.

Microfluidic Device Failure Modes.

The testing of DEP microfluidic devices for this thesis presented an array of challenges related to potential failure points. These were carefully addressed as the experimental process. Often these device failures require multiple tests with and without successful particle detection. Understanding and mitigating these issues were critical for ensuring the reliability and accuracy of the experimental outcomes. This section of the thesis will delve into the various modes of failure encountered in microfluidic devices, which include obstructing bubble formation, solution contamination, PDMS structure deformation, sucrose contamination, virus sample integrity, and BSA (Bovine serum albumin) coating issues.

Clogging of a microfluidic device by obstructing bubbles is a common issue that can interfere with the flow of fluids through the channels, thereby hampering the experimental process. Addressing the main factors leading to clogging and developing effective strategies was paramount as seen in Figure 15. Understanding the nature of these obstructions as PDMS particulates that have been introduced into the system during the fabrication of the DEP devices decreases the likelihood of them interrupting an experiment. Reduction of these obstructions was

done with multiple methods, including increasing the isopropanol washing steps during the cleaning stages of PDMS casts, and using a fresh punch 2mm Picu Punch to create the opening and exit points of the microfluidic channel.

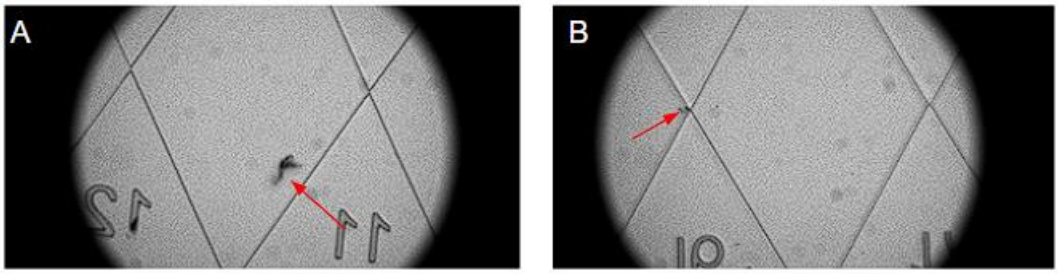

Figure 15 Shows two separate DEP devices with contamination PDMS. Image A is a larger piece of debris that has not yet obstructed the flow of buffer in the device. Image B is a smaller clog wedged in the teeth of the device.

The formation of bubbles within microfluidic channels is another concern as seen in Figure 16. Bubbles can introduce errors in experimental results and affect the reliability of data. Removing or preventing bubble formation requires identification of the sources of the bubble formation after the oxygen plasma bonding process and implementing reduction methods, such as putting the DEP device in a closed container and letting it rest in a 4^{o}C fridge for 5 min.

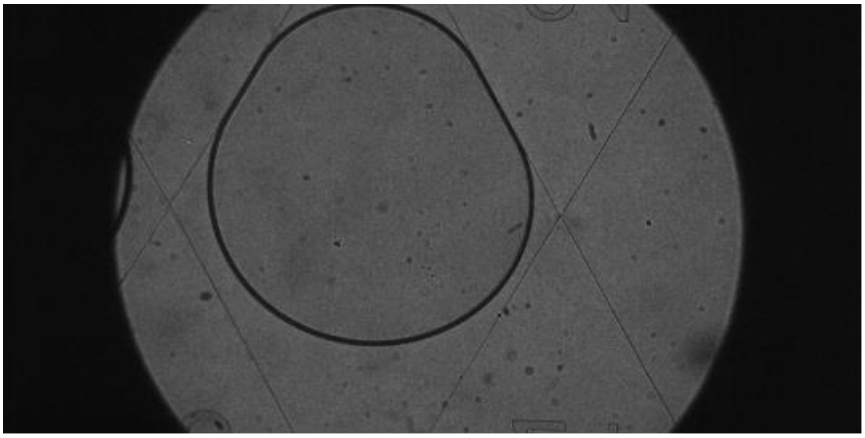

Figure 16 Shows a DEP device with a large bubble inside the microfluidic chamber.

Buffer contamination entering the device, or present in the virus samples themselves, is a critical issue that can compromise the integrity of experiments. Contamination from external sources can lead to misleading or inaccurate results. Reduction of the sources of contamination was addressed by filtration of buffer though 0.22 um filters to remove larger particles above 220 nm in size. It was also necessary to validate that the 18M-ohm water. Additionally, testing the concentration of particles in solution using a particle counter DLS system for particles under the size of the filter is required or is needed to have less than $10^7(\frac{particles}{ml})$ so that the signal to noise ratio of contamination is greater than 10 to 1.

The deformation of PDMS structures in the microfluidic device can impact the device's performance due to the change in electrical fields being directly proportional to the gap size that is created by the insulating material. Identifying the devices that have incorrect gap size as seen in Figure 17 is essential to the proper testing of viral samples.

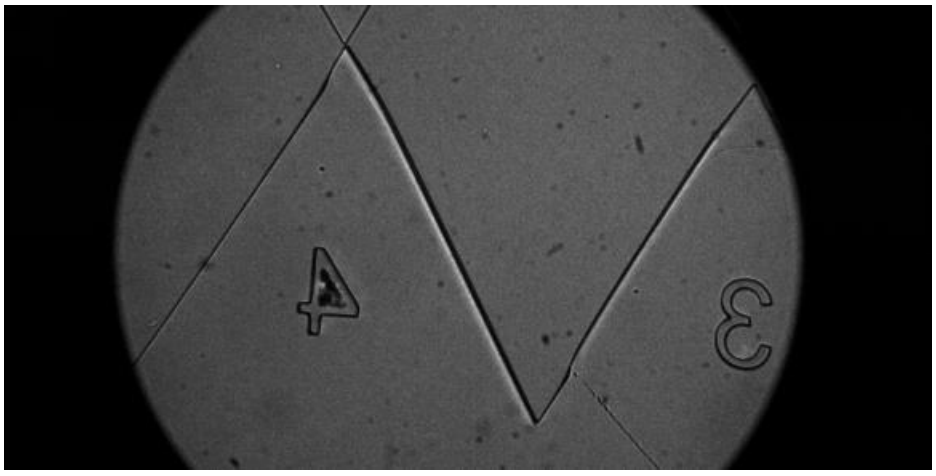

Figure 17. A deformed PDMS casting that lacks straight edges is shown as an example of an alteration that will impact experimental results.

Furthermore, the sensitivity of virus samples to temperature changes during -80°C freeze-thaw cycles, poses a substantial risk to the integrity of samples and concentration accuracy. Reducing or mitigating the extent of sample temperature cycling is necessary and critical for maintaining the integrity of the viral samples being tested. A simple method is to mark

each tube that has experienced a freeze-thaw and removing all tubes that have experienced 3 cycles. Aliquoting samples for single experiment use avoids the need for freeze-thaw cycles.

The presence of long strands of string-like materials within the microfluidic device can also disrupt fluid flow, shed particles and compromise experimental results as seen in Figure 18. One method of reducing the impact of these particles is fabricating the devices within a positive-pressure cabinet with an air filter to reduce the amount of particulate and strands that accumulate during fabrication of DEP devices.

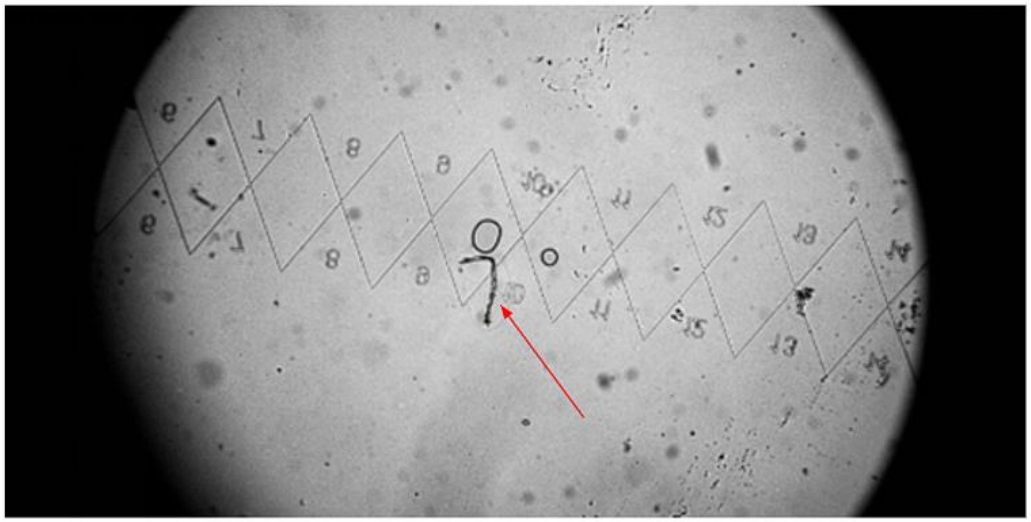

Figure 18. A wide-field image of a DEP device that has a string of unknown material embedded between the glass and PDMS at gate 10 is pointed out with red arrow. Additionally, air bubbles and PDMS debris are seen at the smaller gates.

Lastly, when voltages exceeding DC 2000 V are applied, there is a risk of the device coating being pulled into solution, greatly affecting the experiment's outcomes as seen in Figure 19. For example, Bovine Serum Albumin (BSA) has been used for other DEP experiments as a means of reducing electroosmotic flow increasing the change of trapping of particles.

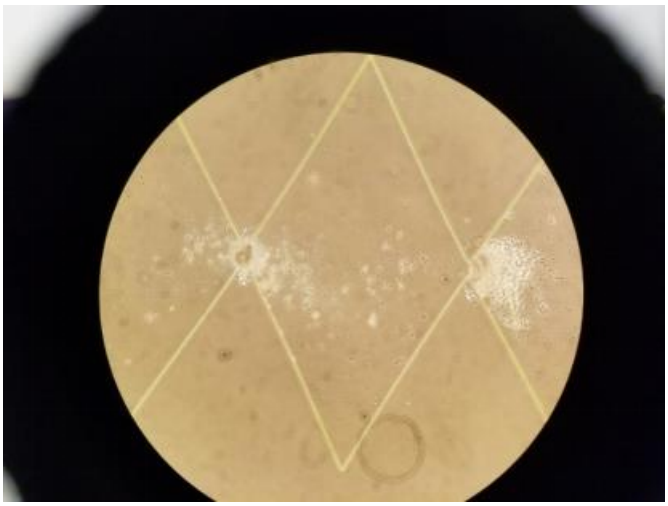

Figure 19. Bright-field image of DEP device after a DEP experiment showing a build-up of BSA clogging inside of the device, after applying 2000V.

In conclusion, the research outline in this section of the thesis gives a brief overview of the various modes of failure that microfluidic devices may encounter and illustrates some of the troubleshooting used to mitigate the risk of device failures. Through these initial 'troubleshooting' experiments, multiple ways to mitigate DEP measurement issues were identified which have the potential to improve reliability and accuracy of microfluidic DEP experiments, ultimately leading to more meaningful and scientifically sound results in a wide range of research domains.

NS300 testing of MHV A59 virus detection

Table 1 below shows data collected for MHV A59 using the NS300 device setup.

Mean	Mode	SD	D10	D50	D90	Particles per frame	Concentration	Confidence
39.8	30.9	22.5	28.8	31.7	73.7	166.1	3.04E+09	1
122.2	111.5	46.4	75.7	111.4	192.8	1.7	3.11E+07	1
148.5	110.6	59.1	91.9	132.3	235	5.6	1.03E+08	1.5
165.5	148.4	86.6	114	144.7	242	8.1	1.08E+08	2
115.6	88.1	49.9	78.6	101.9	222.3	1.4	2.65E+07	2
121	87.5	47.4	75	110.5	173.4	9.4	1.72E+08	3
151.5	112.7	56.2	99.2	137	223.3	122.9	1.01E+09	3.5
176.2	113.8	80.5	106.1	154.7	270.7	122.3	8.83E+08	3.5
171.3	119.8	71.9	104.7	154.2	269.5	122.2	8.94E+08	3.5
117.1	88.8	45.8	84.1	101.1	188.5	5.3	9.72E+07	3.5
127.8	105.6	32.7	99.2	118.4	170	10.9	1.18E+08	4
131.7	111	52.2	95.5	119.8	161.9	28.4	3.77E+08	4
108.9	86.5	39.9	66.8	100.4	160.9	368.2	6.74E+09	4
126.4	107.7	30.3	98.7	117.6	161.8	105.8	9.90E+08	4.5
104.4	98	27.1	76.4	100.9	135.7	72.5	1.24E+09	4.5
99.6	83.2	32.3	76.9	89	134.6	58.6	1.07E+09	5
123	107	30.4	99.4	112.8	159.1	45.5	2.77E+08	5
140	99	60.7	91.5	121.3	214	63.1	4.16E+08	5
119.9	86.3	50.9	81.2	101.5	188.1	46	8.41E+08	5
109.7	87.4	44.1	80.7	94.5	148.4	23.1	4.23E+08	5
102.2	81.9	29.9	77.1	91.8	137.6	122.1	2.23E+09	5

Table 1. The NS300 device was used for 22 measurement results of MHV A59. The table is sorted by confidence in the quality of samples. Red indicates samples that were not used for experiments, yellow highlights samples, used case-by-case for experiments. Green highlights samples used multiple types of experiments.

The information derived from the analysis of Table 1 containing NS300 data, which were rated based on the confidence of the samples, provided valuable insights into the factors influencing the reliability of the results. Confidence was assigned by core users of DLS systems. The table contains several metrics including size, particle count, particles per frame, concentration, standard deviation, D10, D50, and D90, respectively. Particle size, particles per frame, and concentration that were larger had positive correlations with the confidence ratings assigned to the samples.

Size in nm, as a critical metric demonstrated a strong correlation with the level of confidence that an MHV-A59 sample was good for an experiment. Samples closer to the known size range of MHV particles received higher confidence ratings. Contaminaton with other particles such as sugar crystals that were 10nm to 30nm in size, had a negative effect.

The metric for particles per frame also exhibited a correlation with the confidence ratings. Samples with higher particle count per frame meant that more particles were being tested with Brownian motion for the size of the particles. In practical terms, a larger particle count per frame indicates a more comprehensive and representative sample, which is often indicative of a higher quality sample that will result in higher quality data.

Concentration, another key metric in the table, displayed a notable positive correlation with the confidence ratings. Samples with well-defined and higher particle concentrations at $10^8(\frac{particles}{ml})$ or greater produced better, more reliable results. A clear, high concentrated particle population is essential for obtaining reliable and trusted DEP data, as it reduces the likelihood of unsuitable particles or concentrations so low that background noise would drown out all usable results.

In summary, these data sets underscores the significance of size accuracy, a high particle count per frame, and well-defined concentration readings, for better-quality data from DEP experiments. As Nanosight systems are built to test the concentration of diffracting particles within liquid samples, these DEP measurements are intended to dovetail with Nanosight data. Furthermore, these findings emphasize the importance of rigorous quality control and validation processes in microfluidic systems, as it plays a pivotal role in determining if the sample is testable in a defined system.

CHAPTER 3

METHODS

The following protocols describe the MHV A59 and, PENN98 viruses, L2 and 17CL-1 cell lines used for the growth, purification and virus plaque assays for sample preparation for DEP experiments. [18] Unless otherwise noted, all virus growth incubation procedures and plaque assays are performed in a 5% CO_2 incubator at 37°C under BSL2 containment.

MHVA59 virus infection in 17CL-1 cell lines - An overview of the method

17CL-1 cells were grown to confluence in a sterile T-150 Cyto One tissue culture flask with a vented cap. The cells were grown using Dulbecco's Modified Eagle Medium (DMEM) with the addition of 5% volume fetal bovine serum (FBS), 2mM l-glutamine, and 50 gentamicin. Once cell monolayers were 90% confluent, cells were infected with MHV A59 at a multiplicity of infection of 1 (MOI = 1). MHV A59 was transferred to confluent monolayers in Phosphate Buffered Saline with added 3 mM EDTA (PBS), overlaying the cells with 2ml in each T-150 over 1 hour, rocking infected cells every 10 min. The PBS was then replaced with fresh DMEM and the cells were left in an incubator for 24h to allow for viral replication.

Purification of the MHV A59 virus – An overview of the method

Infected cells were collected and the MHV populated DMEM was removed from the T-150 flasks, placed in sterile 50 mL Falcon High Clarity Conical Centrifuge tubes, media was clarified by centrifugation Beckman Coulter Allegra X-22R for 10 min, 4°C, at 1000 X g to pellet the cell debris. All buffers made for the storage or purification of MHV were filtered through a 0.22um filter to remove any external contamination, such as particulates. The DMEM containing MHV collected and placed over a step gradient made with TMEN (50mMol Tris maleate, 100mM NaCl, 10mMol EDTA, at ph 7.2). 70% w/w sucrose base was added to the buffer and a TMEN with 20% w/w sucrose added on top, this is performed in 37 mL Beckman Coulter Ultra-Clear

Centrifuge tubes. A more in-depth instruction on how to specifically create gradients is available in a Sindbis purification guide, and can be adjusted for sucrose. [19] The step gradient is spun at 100,000 g, 4°C for 4 hours in a Beckman Coulter ultracentrifuge. The two layers of sucrose capture the MHV between them and the majority of the TMEN above the 20% sucrose layer is discarded and the layer between the sucrose bands is retained. The captured sample is placed over a 20-70% linear sucrose gradient created using a Buchler Instruments Auto Densi-Flow to create a linear gradient. The linear gradient is spun at 100,000 g, 4°C for 16 hours, with the MHV that has been fractionated from the centrifuge tube. The MHV in TMEN and sucrose is put through dialysis with 1 L TMEN at 4°C using Float-A-Lyzer G2 Dialysis Device, and replacing the 1L TMEN after 1 h to remove sucrose from solution. Samples are stored in TMEN at 80°C in aliquot's of 10ul, 50ul and 100ul.

MHV A59 Plaque assays - An overview of the method

Characterization of the purified MHV sample began with a plaque assay that follows the same procedure as described in the following protocols. [18] An overview of the plaque assay methodology is as follows; L2 cells are grown until confluent in CytoOne 6-well Multiwell plate with lid. When L2 cells are confluent thaw the MHV samples in a 37°C water bath. When MHV samples are thawed, place samples on ice, and dilute the virus in PBS serially, in ten fold increments. The virus dilutions are kept on ice to prevent heat damage to the sample. Remove media from 6 well plates and wash with PBS. Overlay well plates in triplicate with pre-made dilutions of MHV in PBS, rocking by hand every 10 min for one hour. Place DMEM into a 50°C water bath, melt 2% agarose in the microwave and let cool between 45 °C and 50°C. Mix equal volumes of DMEM and agarose to overlay each well and gently tilt the plate to completely cover the cells. Let plates sit until agarose has solidified. Place the plates into the incubator at 37°C for 2 days. Agarose is removed after 2 days, and the plates are stained with 0.1% crystal violet and 70% ethanol. Count the plaques using a light box to illuminate the cleared section of cells in the

well plates. Calculate the pfu/ml by using the average plaque count from 3 wells x 10 x the dilution factor.

Dynamic Light Scattering (DLS) - An overview of the method

DLS was used to identify the concentration and size distribution of intact viruses. The measurements were taken with a Malvern Instruments Nanosight 300 with a 50 mW 532 nm green ribbon laser. The experiments were performed using serial dilutions by factors of 10 with 1 mL of sample for each dilution. Using a syringe, the dilutions are pushed through the microfluidic cell and removing any bubbles getting trapped within the device. TMEN was tested first to identify any points of contamination in the buffer or in the Nanosight. The TMEN buffer was tested with 60 second long videos where the samples were pushed through the device after each video. The MHV samples were tested with 5, 60 second long videos. The settings used were camera level 12 and detection threshold of 4 during the analysis of the Brownian motion of the particles.

Electron microscopy (EM) - An overview of the method

EM imaging was carried out using Tecnai F20 TEM onto Carbon 300 mesh, copper grids from Electron Microscopy Sciences with 5 ul of Viral samples and negatively stained with 2% uranyl acetate. The images then are collected and saved in a .TIF format.

DEP device fabrication – An overview of the method

DEP devices are created by PDMS casts using the experimental procedures described below. [3] An overview of the creation of PDMS casts is described. The following casting is done in a positive pressure heap filter working box. PDMS is created using Silicone Elastomer Kit by poring over PDMS and 10% of the supplied hardener onto a silicon wafer with the desired embossed microfluidic DEP device as described in figure 4. The PDMS is placed in a vacuum chamber to remove all extra air bubbles from the PDMS and hardener solution over 10 min. The PDMS wafer is baked at 80°C for one hour, then the PDMS microfluidic chamber is removed from the silicon embossed wafer. 22 mm by 44 mm coverslips are washed 3 times following acetone,

isopropanol, water then sonicated for 30 seconds. The PDMS microfluidic chamber is washed 3 times with isopropanol, water, and sonication is limited to 10 seconds. The PDMS microfluidic chamber and coverslips are air dried before being placed in a Zepto Plasma Lab System for oxygen plasma bonding to fuse the coverslip and PDMS device. Following oxygen plasma bonding contact bonding is done then the microfluidic DEP device is filled with 10 ul of DEP buffer (0.3 M Sucrose, 5 mM MES, 7.2 pH, conductivity 330 s/cm). The use of scotch tape stuck to the PDMS top of the device and gently removed can reduce dust on top of the device. Conducted a bright field inspection to identify any clocks or failures in the making of the microfluidic device.

DEP device testing – An overview of the method

The device is then placed on the Hayes Diagnostic Incorporated Custom laser scatter system using 3 red lasers (100 mw 663 nm) for illumination. Platinum electrodes are inserted into the outlets of the DEP device and connected to DC power supply. Labsmith HSV3000 images were then collected over 30 second intervals, with 10 seconds without voltage followed by 10 seconds of applied voltage. The DC voltage is increased by steps of 200V until reaching 800V. The previous process used for data collection is then repeated after the device is loaded with 10 ul MHV with a concentration of 10^8 Particles/ml. Analysis of the image stack is completed using National Institutes of Health *ImageJ* to pull off individual frames during the experiment.

Comparison of MHV and PENN98 spike proteins

A Python code was utilized for aligning and comparing the spike protein of A59 and PENN98 with a spike protein from MHV-2.[23] The Python code, which is available in Appendix A, was used for this purpose. The Python code worked by tracking the genome sequence by sequence and comparing the changes over the total length of the genome and creating a percentage difference.

Sindbis DNA transformation protocol An overview of the method

The following protocols describe the Sindbis Virus Heat Resistant (SVHR), Sindbis Virus Venus(SVV), and Sindbis Virus Venus Tetracycteine(SVVT) and the cell lines, BHK-21 cell line ATCC #CCL10 used for the growth, purification and virus plaque assays used in this experiment. [24] The SVHR, SVV, and SVVT DNA was procured from Tuli Mukhopadhyay at Indiana University Bloomington. Unless otherwise noted, all virus growth procedures are performed in a 5% CO_2 incubator at 37°C under BSL2 containment.

The provided set of instructions outlines a protocol available with Catalog #200314 XL-10 ultra-competent cells from Agilent Technologies using Escherichia coli(E.coli) cells Here is a step-by-step summary of the procedure. [25] To initiate the bacterial transformation process, start by pre-chilling two 14-ml BD Falcon polypropylene round-bottom tubes on ice. It's important to note that one of these tubes will be designated for experimental transformation, while the other will serve as the pUC18 control. Simultaneously, preheat the NZY+ broth to 42°C for subsequent steps.

Thaw the E. coli cells meticulously on ice. Once the cells are fully thawed, gently mix them and aliquot 100 µl of the cells into each of the chilled tubes. Following this, add 4 µl of the β-Mercaptoethanol (β-ME) mix, provided in the kit, to each aliquot of cells. Give the tubes a gentle swirl to ensure proper mixing and subsequently incubate the cells on ice for a duration of 10 minutes. During this incubation, it is important to swirl the tubes gently every 2 minutes to facilitate optimal conditions for the subsequent steps.

Next, add 0.1-50 ng of the Sindbis DNA to one of the aliquots of cells. Following the addition of DNA, gently swirl the tubes to ensure thorough mixing and rest the samples on ice for a period of 30 minutes. To complete this stage of the transformation, heat pulse the tubes by immersing them in a 42°C water bath for precisely 30 seconds.

After the heat pulse, rest the tubes once again on ice for an additional 2 minutes to cool down and stabilize the cells for the subsequent steps. Following these preparatory steps, add 0.9 ml of preheated to 42°C NZY broth to each tube and incubate the tubes at 37°C for 1 hour. During this incubation period, ensure that the tubes are subjected to shaking at a speed of 250 rpm to aid in the recovery of the transformed cells.

Once the incubation period is completed, it's time to plate the transformation mixture. Plate a volume of ≤200 µl of the transformation mixture onto LB agar plates that contain the appropriate antibiotic. To allow the bacterial colonies to form and develop, incubate the plates at 37°C overnight.

In terms of expected outcomes, for the pUC18 control transformation, anticipate the growth of approximately 250 colonies, with a projected count of $\geq 5X10^9$ colony-forming units per microgram (cfu/µg) of pUC18 DNA. The Sindbis DNA, the number of colonies will exhibit variations according to the size and form of the transforming DNA, with larger and non-supercoiled DNA typically yielding fewer colonies.

Mini Prep - An overview of the method

QIAgen miniprep Mini prep used to isolate Sindbis DNA from bacteria follows the protocol supplied. To initiate the mini-prep procedure, start by inoculating 5 ml of bacterial culture obtained from Sindbis transformation protocol. Once inoculated, divide 3 ml of this culture into two separate 1.5 ml micro-centrifuge tubes. These tubes are then subjected to a brief centrifugation on a tabletop centrifuge, spinning for 1 minute at 13,000 rpm. The supernatant is carefully discarded, and the cell pellets are resuspended in 125 µl of P1 buffer.

Following the resuspension, 250 µl of P2 buffer is added to each tube, and the contents are gently mixed by inverting the tubes six times. It's crucial to ensure that this step does not exceed more than 5 minutes. Subsequently, 350 µl of N3 buffer is added to each tube, and

immediate mixing is performed by inverting the tubes six times. If a pH indicator was incorporated into the P1 buffer, the solution should become colorless at this point. To separate the cellular debris from the solution, the tubes are centrifuged for 10 minutes at 13,000 rpm. The supernatant from this step is then carefully applied to a QIAprep spin column.

The QIAprep spin column is centrifuged for 1 minute at 13,000 rpm, and the flow-through is discarded. The column is subsequently washed by adding 750 µl of buffer PE, and another centrifugation for 1 minute at 13,000 rpm is performed. The flow-through is once again discarded, and an additional 1-minute centrifugation ensures the removal of any traces of the PE buffer from the column.

The final step involves transferring the QIA spin column to a new 1.5 ml microcentrifuge tube. To elute the plasmid, 50 µl of either water, EB buffer containing EDTA, or TE buffer is added to the column. After letting the tube stand for 1 minute, a final centrifugation for 1 minute at 13,000 rpm is performed to facilitate the elution process, yielding the desired plasmid DNA.

Capped RNA synthesis of Sindbis virus's

RNA synthesis of Sindbis virus was completed using New England Biolabs Capped RNA Synthesis (E2040) protocol. [27] The Capped RNA synthesis protocol was initiated by thawing the required kit components, which were then mixed and pulse-spun in a microfuge to ensure that the solutions collected at the bottom of the tubes. These prepared components were diligently kept on ice throughout the procedure.

A 10 mM GTP solution was generated by diluting an aliquot of 50 mM GTP at a 1:5 ratio with nuclease-free water. The cap analog was prepared at a concentration of 40 mM, ensuring that it was ready for the subsequent steps.

The reaction was assembled at room temperature by following a precise order: Nuclease-free water was the starting point, followed by the addition of SP6 Reaction Buffer (10X), ATP (50

mM), UTP (50 mM), CTP (50 mM), GTP (10 mM), Cap Analog (40 mM), Sindbis DNA, and the SP6 RNA polymerase Mix. With a total reaction volume of 25ul.

The components of the reaction were mixed thoroughly to achieve a proper combination, and pulse-spin was employed to enhance their uniform distribution. Subsequently, the reaction was incubated at 37°C for a duration of 30 minutes to facilitate the RNA synthesis process.

Electroporation of Sindbis RNA into BHK cells- an overview of the method

The electroporation of RNA into BHK-21 cells protocol was executed following the protocol described below: First, for each T-75 flask, the growth media was aspirated, and the cells were rinsed with 5 mL of warm 1X PBS. After rinsing, the PBS was removed, and 1 mL of trypsin was added to each flask, which was gently rocked to ensure even distribution over the cells. Following a 1- 2 min incubation, the flasks were tapped to release the cells, and 10 mL of cold MEM+++/5% FBS was added to resuspend the cells, with particular emphasis on not pre-warming the media.

The cells were then pipetted into a sterile conical tube and centrifuged at 3000 rpm for 5 minutes at 4°C. This centrifugation step was repeated, and simultaneously, the RNA transcript(s) were thawed on ice. The supernatant was aspirated, and the cells were resuspended in 0.5 mL of cold 1X PBS for each T-75 flask initially used, using a gentle pipetting action.

Subsequently, 0.5 mL of the cell suspension was added to cuvettes with a 2 mm (0.2 cm) gap width, ensuring that the cuvettes had the longer chamber length to accommodate the entire 500 µL between electrodes. Approximately 20 µL of RNA transcript was transferred to the cuvette with the cells, and the samples were pulsed three times using the Bio-Rad GenePulser System set to 1.5 kV (voltage), 25 µF (capacitance), and 2000 ohms (resistance).

After electroporation, the cuvettes were incubated at room temperature in a TC hood for 10 minutes. A 60 mm dish was then filled with 4 mL of MEM+++/5% FBS, with pre-warming being

acceptable in this step. Using a sterile Pasteur pipet attached to a pipet-aid, approximately 1 mL of MEM+++/5% FBS was extracted from the 60 mm dish and added to the cells in the cuvette. Gentle pipetting was employed to break up cell clumps, and all cells were transferred to the 60 mm dish already containing approximately 3 mL of MEM+++/5% FBS. The resulting mixture was then incubated in a 37°C incubator as required for the experiment.

Sindbis Virus infection in BHK-21 cell lines - An overview of the method

The following protocol was based off protocols from Sindbis Virus: Propagation, Quantification, and Storage. [24] BHK-21 cells were grown to confluence in a sterile T-150 Cyto One tissue culture flask with a vented cap. The cells were grown using Modified Eagle Medium (MEM) with the addition of 5% volume fetal bovine serum (FBS), 10% TPP Broth, 2.4mM l-glutamine, and 50 gentamicin. Once cell monolayers were 90% confluent, cells were infected with the different assembled Sindbis Virus's at a multiplicity of infection of .1 (MOI = 0.1). Sindbis was transferred to confluent monolayers in Phosphate Buffered Saline with added 3 mM EDTA (PBS), overlaying the cells with 2ml in each T-150 over 1 hour, rocking infected cells every 10 min. The PBS was then replaced with fresh MEM and the cells were left in an incubator for 24h to allow for viral assembly.

Sindbis Virus Purification

The following protocol is very similar to the steps outlined in MHV virus purification, with some differences in buffers, gradients and spin speeds, the three viruses were purified in the same manner a detailed protocol can be found in references. [19] Infected cells were collected and the Sindbis viruses populated MEM was removed from the T-150 flasks, placed in sterile 50 mL Falcon High Clarity Conical Centrifuge tubes and clarified by centrifugation for 10 min, 4°C, at 1000 X g to pellet the cell debris. All buffers made for the storage or purification of MHV were Filtered through a 0.22 um filter to remove any external contamination. The MEM containing Sindbis was collected and placed over a step gradient made with PN (100mM NaCl, 50mM

PIPES, at ph 6.5). 35% w/w potassium tartrate base was added to the buffer and a PN with 15% w/w potassium tartrate added on top, this is performed in 37 mL Beckman Coulter Ultra-Clear Centrifuge tubes. A more in-depth instruction on how to create gradients is available in a Sindbis purification guide. [19] The step gradient is spun at 27,000 g, 4°C for 12 hours in a Beckman Coulter ultracentrifuge. The two layers of sucrose capture the MHV between them and the majority of the PN above the 15% potassium tartrate layer is discarded and the layer between the Potassium Tartrate bands is retained. The following retained sample is placed over a linear gradient created between a 35% Potassium tartrate PN solution and 15% potassium tartrate solution using a Buchler Instruments Auto Densi-Flow to create a linear gradient. The linear gradient is spun at 27,000 g, 4°C for 6 hours, with the Sindbis that has been fractionated from the centrifuge tube. The Sindbis in PN and potassium tartrate is put through dialysis with 1 L PN at 4°C using Float-A-Lyzer G2 dialysis cassettes and replacing the 1L PN after 1 h to remove sucrose from solution. Samples are stored in PN at 80°C in aliquot's of 10 ul, 50 ul and 100 ul.

CHAPTER 4

RESULTS

MHV Results

MHV-A59 and PENN98 was characterized for infectivity, size, size distribution, and concentration after purification was completed. DLS was completed for the TMEN buffer without and with virus samples to determine specifically the concentration and size distribution of the purified virus as shown in Figure 20. Five videos of MHV were collected on the Nanosight 300 with the average concentrations displayed against the averages of the TMEN alone videos.

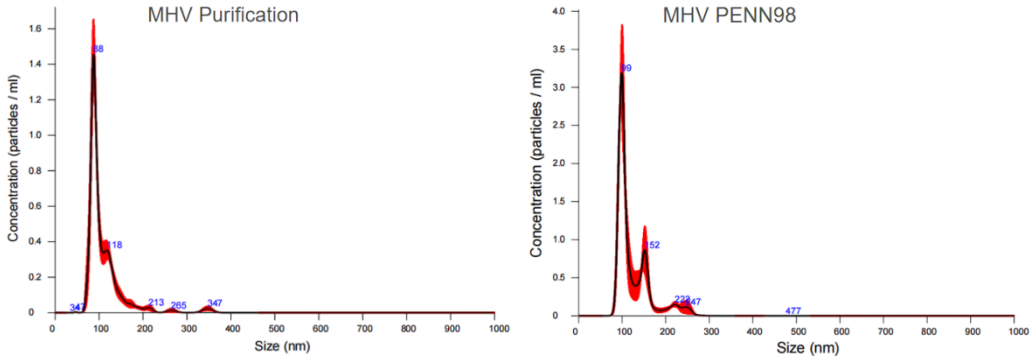

Figure 20. Graphs of the size distribution of MHV-A59 (left) taken from the NS300, with the peak of the concentration for MHV reading at 89 nm. PENN98 (right) with a peak of 99 nm, and a secondary peak at 152 nm.

The total concentration of particles within the MHV A59 sample was found to be $4.2X10^{11}$ particles/ml accounting for a dilution of 1/1000 the particle distribution had a mean of 110 nm. The TMEN control had a total concentration of $5X10^{6}$ particles/ml. The size distribution of the particles clustered near 88 nm with a relatively small secondary peak 118 nm. PENN98 had a concentration of $9.7X10^{11}$ particles/ml after the same dilution as A59 with a mean of 124 nm.

TEM images of the MHV particles can be seen in Figures 19 & 20 to visually determine the integrity of particles after purification. The shapes of the virus particles do not show major structural deviations, no major contaminations of other materials, and demonstrates a monodisperse collection of MHV A59 particles in agreement with the Nanosight results.

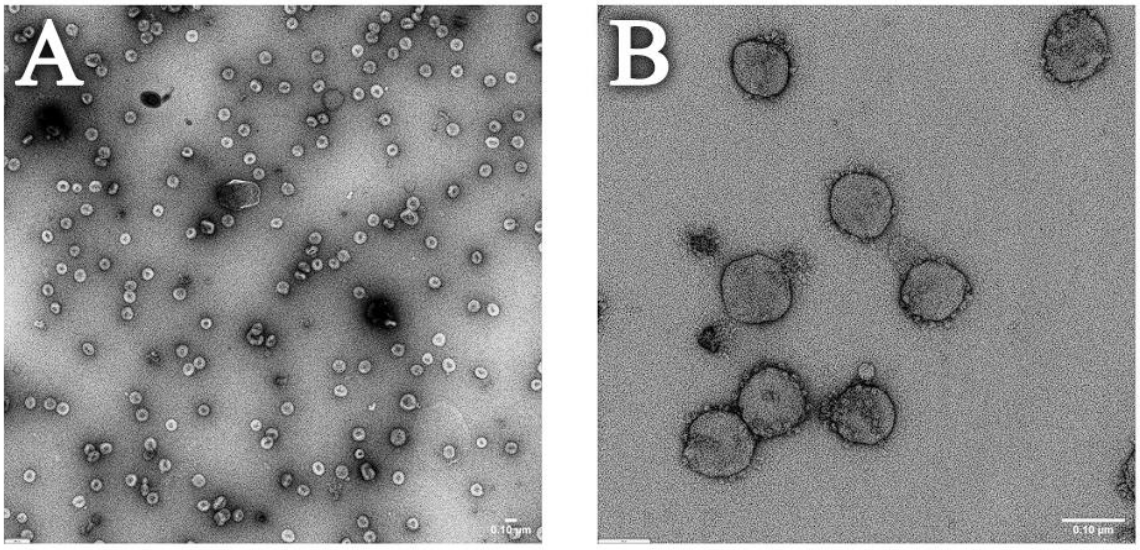

Figure 21. A TEM image of the MHV A59 negative stained with 2% uranyl acetate. Image A is a zoomed-out image of the virus particles, image B is a close up of 8 MHV particles with spike proteins visible. EM images were taken and kindly provided by Bereket Estifanos in the Hogue Lab.

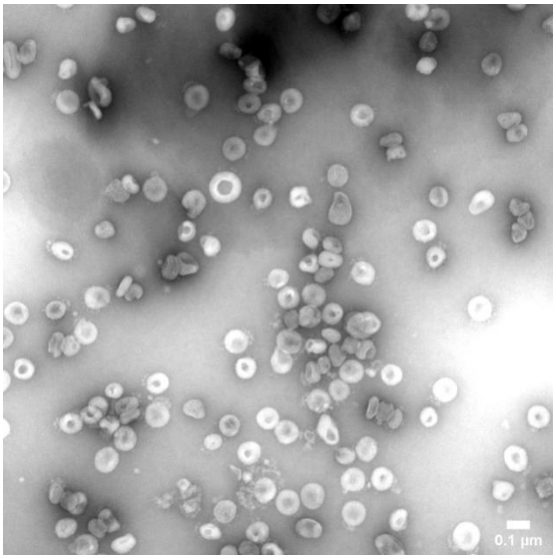

Figure 22. A TEM image of PENN98 negative stained with 2% uranyl acetate. EM images were taken and kindly provided by Bereket Estifanos in the Hogue Lab.

The plaque assay demonstrated $1X10^{10}$ pfu/ml of MHV A59, lower than what was detected by the DLS testing by more than an order of magnitude. Plaque assays measure the number of infectious particles, whereas DLS measures total particles, regardless of whether the particles are infectious. Either the difference between DLS and plaque assay measurements

likely reflect particles that are not infectious or contaminating material or paraticles in the samples.

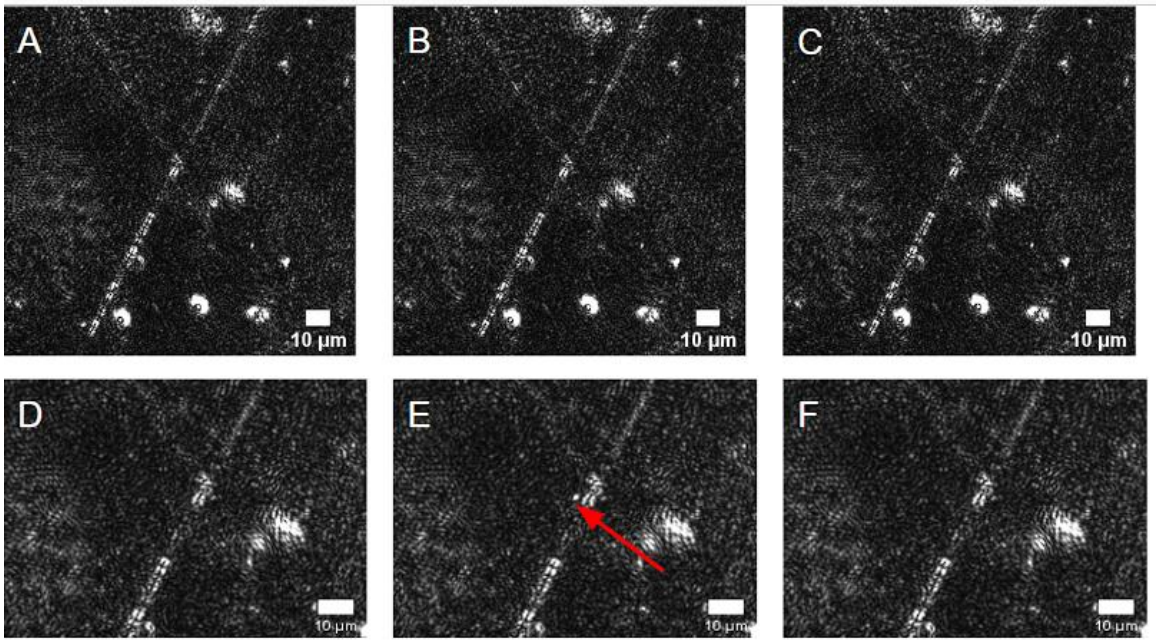

Figure 23. Visual comparison of TMEN then MHV A59 samples in the same DEP device focused on teeth that have a 3um gap. The positive dc voltage is applied to the left of the images and the negative to the right. (A) TMEN under 0V in a DEP device. (B) TMEN under 800V in a DEP device for 10 seconds. (C) TMEN under 0V in a DEP device after 800V is returned to 0V. (D) MHV under 0V in DEP devices. (E) MHV A59 under 800V in a DEP device for 10 seconds, included red line to show bright spot of a particle stopped at gate. (F) MHV A59 under 0V in a DEP device after 800V is returned to 0V.

MHV A59 was inserted into the same DEP device as the TMEN demonstrating minimal particle count before the addition of the virus particles. The effects of the electric field applied across the device are evident as the particles begin streaming from left to right across the DEP device, with particles in TMEN passing though all 3 visible gates. The MHV A59 sample show particles slowing down and looping around the left side teeth labeled 22 and 23. The 3 um gap was used for testing as it had the largest electrical field gradient in this device, with the gradient field being increased by increasing the voltage to 800 V.

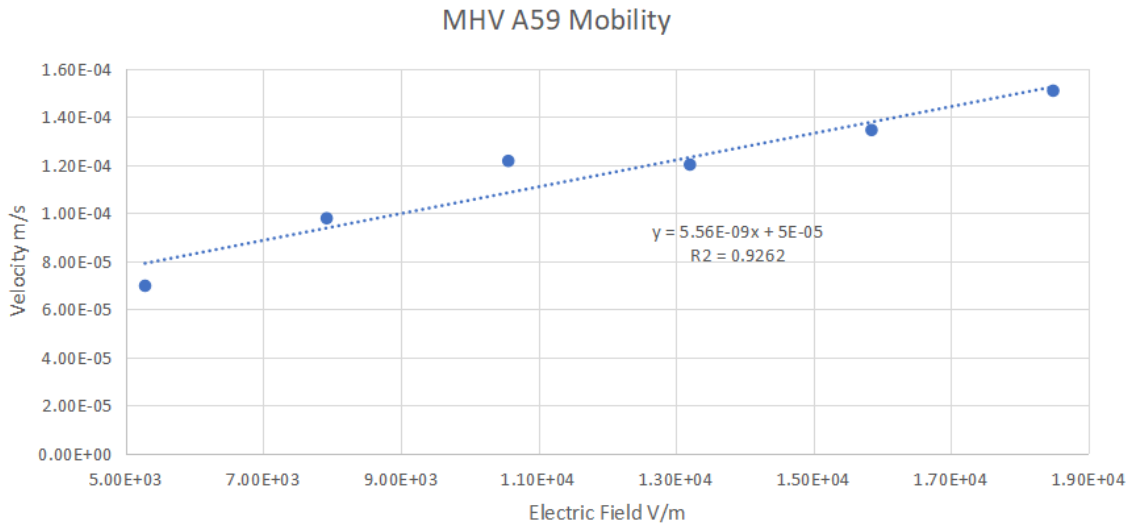

Figure 24. Plot of the MHV A59 particle's velocities against the electric field to determine the μ_{EK} of 5.56X10^{-9}($\frac{m^2}{Vs}$).

With the information gained before the MHV A59 was captured, it was possible to determine the μ_{EK} of 5.56X10^{-9} $\left(\frac{m^2}{Vs}\right)$ by measuring the velocities of MHV A59 particles as they passed through the microfluidic device and the electric field as the voltage increased across the device for subsequent data points. With a capture of MHV-A59 at of 800V and a DEP buffer conductivity of 334 $\frac{S}{cm}$ the E_{KMr} in a DEP device is 7.82 X 10^{11} $\frac{V}{m}$. Following the equation (3) found in DEP Fundamentals μ_{DEP} is calculated to be 7.11X10^{-21}($\frac{m^4}{V^2 S}$) for this data set.

Sindbis Results

The Sindbis vVirus was characterized for size, size distribution, fluorescence, and concentration after purification of virus particles was completed. DLS was completed on both the PN buffer without and with virus as described above for MHV A59 to determine specifically the concentration and size distribution of the purified virus stocks used. Results are shown in Figure 24 in comparison with to the control of PN media alone.

Three videos of Sindbis were collected on the Nanosight 300 apparatus with the average concentrations displayed against the averages of the TMEN videos. As seen in Figure 25 the BHK-21 cells were infected with SVV, and the replication of live virus was demonstrated by the virus-encoded Venus fluorescence marker within the cells during the infection.

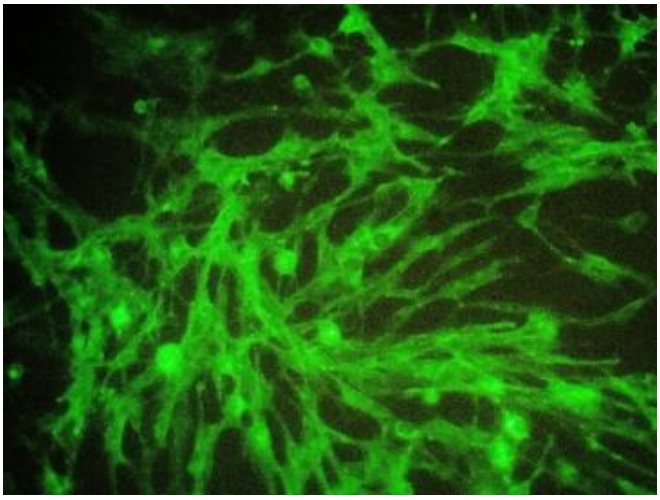

Figure 25. BHK-21 cells infected with Sindbis virus Venus (SVV) under EVOS FL Auto Life technologies green fluorescence scope, viewing successful fluorescence incorporation during replication.

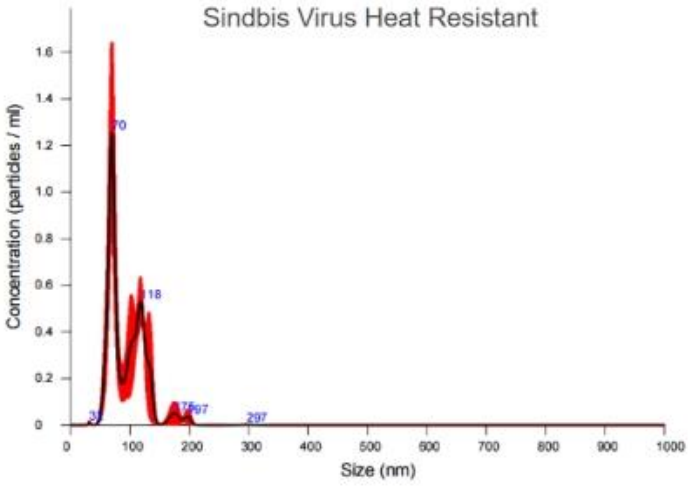

Figure 26. SVHR virus DLS results from NanoSight 300 apparatus with a primary peak of 70nm in size, and a secondary peak at 118nm.

SVHR viral samples, as assessed under DLS with the NS300 apparatus, were found to have a concentration of 3.94X10^{10} particles/ml based on a dilution of 1/100, with a mean size of 94 nm, the primary peak of sample is 70nm closely matching known structure. As seen in Figure 26 the size distribution is focused on 70 nm peak with a secondary population peak of 118 nm. PN Buffer was seen to have a particle concentration of 9.49X10^{6} particles/ml.

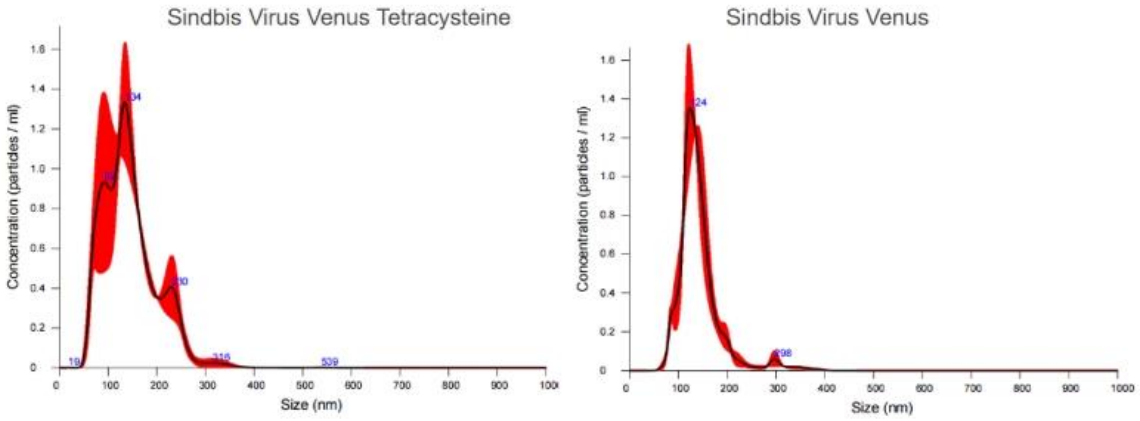

Figure 27 SVVT and SVV DLS results from NS300 with a peak of 134nm in size for SVVT, and a secondary peak at 92nm ~~where as~~whereas SVV has a peak of 124nm.

SVVT viral samples under DLS were found to have a concentration of 1.42X10^{11} particles/ml according to a dilution of 1/100, with a mean of 144 nm. As seen in Figure 25 the size distribution is larger and more spread out when compared to SVHR and SVV. Results from SVV viral samples under DLS were found to have a concentration of 8.47X10^{10} particles/ml according to a dilution of 1/100, with a mean of 142 nm.

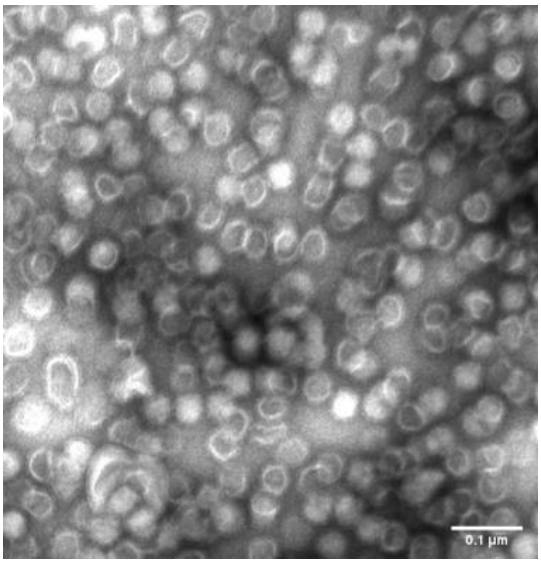

Figure 28. SVHR TEM images showing SVHR particles with an average size diameter of 70nm. EM images were taken and kindly provided by Bereket Estifanosin the Hogue Lab.

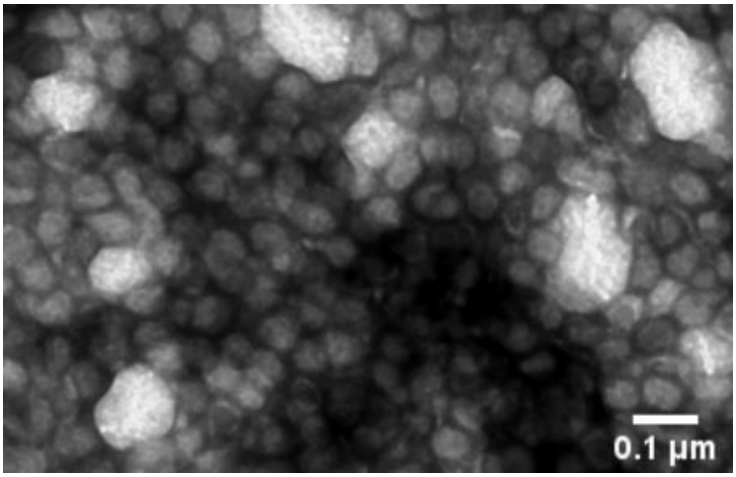

Figure 29. SVVT TEM images visualizing viral particles, and larger clumps of vesicles increasing in size to 200nm diameter. EM images were taken and kindly provided by Bereket Estifanos in the Hogue Lab.

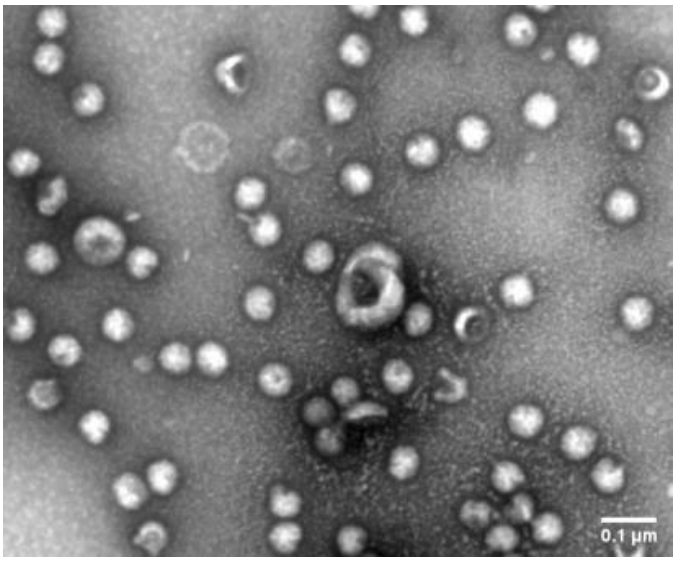

Figure 30 SVV TEM images showing virus particles, with some larger 200nm in size vesicles and other viral particles that have broken down to crescent shapes. EM images were taken and kindly provided by Bereket Estifanosin the Hogue Lab.

Figures 28-30 illustrate TEM imaging of Sindbis virus and mutants with varying ranges in size (Diameters) after purification, matching the size distributions seen within DLS results. In particular, the larger vesicular-like particles can be seen in SVVT in Figure 29. The samples are primarily all Sindbis particles around 70 nm but with variations in size distribution. DEP results have not been fully explored due to initial visualization problems with the NS300 System as seen in Figure 9 from Chapter 2.

CHAPTER 5

CONCLUSIONS

Capture of MHV A59 particles in a DEP device shows promise of this method of separation and detection for application to other viruses and bioparticles. The capture of MHV at 800 V in 10 seconds is a large improvement over other methods such as plaque assay that takes multiple dates to complete. The discrepancy between the results of the plaque assay and the DLS results can be explained in that it measures infectious particles, plaque forming units (pfu). If the sample contains noninfectious particles or other contaminating particles these will not be measured. DLS on the other hand measures total particles, regardless of infectivity. The DEP method can be improved for detection of virions by using better methods of boosting the visibility of the particles near gates though optimized laser light scattering or post processing of gathered data.

CHAPTER 6

DISCUSSION

The research and development outlined in this thesis has paved the way for promising future experiments and technology developments that will significantly advance the utility of virus detection using DEP microfluidic devices. In this thesis, the DEP technique was further refined and optimized to the point where we can visualize and characterize the physical properties of MHV A59. The next steps of this research should focus on two main aspects: the development of methods to physically extract virus samples from a microfluidic device after the initial separation for further analysis of the exact identity of the captured virus particles and, secondly, a broader range of virus samples beyond Sindbis, PENN98, MHV A59 should be tested. Direct comparison of MHV A59 and MHV PENN98 should be done. The long-term goal will be to assess whether the DEP technology can separate more closely related viral mutants that otherwise have very similar virion physical characteristics. In practical terms, a major outcome would be to determine what extend DEP technology could be used to assess virus evolution as measured by mutational drift in real time.

First and foremost, the ability to extract the DEP separated virus samples from within the microfluidic device is a critical step in enhancing the practicality, efficiency, and validation of this technology. Currently, microfluidic devices offer remarkable advantages in terms of rapid low-cost and sensitive virus detection but often lack the capability to recover virus samples for further analysis. Developing efficient methods for sample retrieval will enable us to perform additional studies, such as TEM for the identification of structural changes due to the effects of electrical field gradients, plaque assays to identify whether the viral samples are still infectious, genomic sequencing analysis to assess for genetic mutations, and any other testing that can be instrumental in understanding the virus behavior, mutations, and response to DEP forces within this microfluidic device.

Additionally, expanding our research to include a more diverse range of virus data points is essential. Viruses are known for rapid acquisition of mutations, and various genetic factors can induce structural changes or genetic mutations that can affect the virion structure. For example, point mutations that alter amino acid charge of any virion structural protein would be expected to alter DEP mobility. By testing a broader spectrum of viruses including those described in this thesis, with various amounts of structural changes and genetic changes we can better assess the versatility, adaptability, and limitations of DEP devices for virus detection. These steps not only enhance the understanding of DEP for particles under 1 micron in size but could also contribute to the understanding and reliability of the technology to identify viruses in general.

Furthermore, the ability to separate different biological samples using DEP microfluidic devices has a number of implications as the technology matures. For example, blue laser light was optimal for the illumination and detection of the viruses studied in this thesis, but further testing of other laser light frequencies and power levels is warranted. Beyond virus detection, these devices with more development can potentially be utilized in various applications such as point-of-care diagnostics, environmental monitoring of viruses found in plants and animals, or even potentially the detection of virus in clinical biopsies. Eventual miniaturization of a rapid accurate and efficient diagnostic DEP virus detection system has broad potential. The capability to efficiently, rapidly, and accurately separate distinct biological samples, whether they are viruses, cells, or other bioparticles such as exosomes, can lead to advancements in healthcare, any system affected by viral infections, and biological research.

The next steps in this research are pivotal for advancing DEP microfluidic-based virus detection and for other biotech applications. The ability to remove virus samples from the microfluidic device and test a broader range of virus data points will enhance the understanding of virus structural changes, fundamentals of DEP, and the DEP's microfluidic technology's capabilities and limitations. Furthermore, the ability to separate different viral samples presents a promising avenue for numerous fields, as the capabilities and limitations of this technology continue to be explored.

REFERENCES

[1] “SARS-COV-2 Variant Classifications and Definitions.” *Centers for Disease Control and Prevention*, Centers for Disease Control and Prevention, www.cdc.gov/coronavirus/2019-ncov/variants/variant-classifications.html.

[2] Koerner, Robert W., et al. "Of mice and men: the coronavirus MHV and mouse models as a translational approach to understand SARS-CoV-2." *Viruses* 12.8 (2020): 880.

[3] Ding, Jie, et al. "Concentration of Sindbis virus with optimized gradient insulator-based dielectrophoresis." *Analyst* 141.6 (2016): 1997-2008.

[4] Lecoq, Hervé. "Discovery of the first virus, the tobacco mosaic virus: 1892 or 1898?." *Comptes rendus de l'Academie des sciences. Serie III, Sciences de la vie* 324.10 (2001): 929-933.

[5] Cheng, Xuanhong, Grace Chen, and William R. Rodriguez. "Micro-and nanotechnology for viral detection." *Analytical and bioanalytical chemistry* 393 (2009): 487-501.

[6] Russell, W. C. (1962). A sensitive and precise plaque assay for herpes virus. *Nature*, *195*(4845), 1028-1029.

[7] Zhu H, et al. PCR past, present and future. Biotechniques. 2020;69:317–25.

[8] Peruski AH, Peruski LF (2003) Clin Diagn Lab Immunol 10:506–513

[9] Ghasemi, Somaye, Narges Nazari Harmooshi, and Fakher Rahim. "Diagnostic utility of antigen detection rapid diagnostic tests for Covid-19: a systematic review and meta-analysis." *Diagnostic Pathology* 17.1 (2022): 36.

[10] Goldsmith, C. S., & Miller, S. E. (2009). Modern uses of electron microscopy for detection of viruses. *Clinical microbiology reviews*, *22*(4), 552-563.

[11] Stetefeld, Jörg, Sean A. McKenna, and Trushar R. Patel. "Dynamic light scattering: a practical guide and applications in biomedical sciences." *Biophysical reviews* 8 (2016): 409-427.

[12] Pohl, Herbert A. "The motion and precipitation of suspensoids in divergent electric fields." *Journal of applied Physics* 22.7 (1951): 869-871.

[13] A. Gencoglu, D. Olney, A. LaLonde, K. S. Koppula and B. H. Lapizco-Encinas, *Electrophoresis*, 2014, **35**, 362–373

[14] Pysher, Michele D., and Mark A. Hayes. "Electrophoretic and dielectrophoretic field gradient technique for separating bioparticles." *Analytical chemistry* 79.12 (2007): 4552-4557.

[15] Hayes, Mark A. "Dielectrophoresis of proteins: Experimental data and evolving theory." *Analytical and bioanalytical chemistry* 412 (2020): 3801-3811.

[16] Nakano, Asuka, and Alexandra Ros. "Protein dielectrophoresis: Advances, challenges, and applications." *Electrophoresis* 34.7 (2013): 1085-1096.

[17] Lapizco-Encinas, Blanca H., et al. "Dielectrophoretic concentration and separation of live and dead bacteria in an array of insulators." *Analytical chemistry* 76.6 (2004): 1571-1579.

[18] Leibowitz, Julian, Gili Kaufman, and Pinghua Liu. "Coronaviruses: propagation, quantification, storage, and construction of recombinant mouse hepatitis virus." *Current protocols in microbiology* 21.1 (2011): 15E-1.

[19] Hernandez, Raquel et al. “Purification and Proteomic Analysis of Alphavirus Particles from Sindbis Virus Grown in Mammalian and Insect Cells.” *Bio-protocol* vol. 9,10 e3239. 20 May. 2019, doi:10.21769/BioProtoc.3239

[20] De Carlo, Sacha, and J. Robin Harris. "Negative staining and cryo-negative staining of macromolecules and viruses for TEM." *Micron* 42.2 (2011): 117-131.

[21] Gross, Andreas J., and Thomas RW Herrmann. "History of lasers." *World journal of urology* 25 (2007): 217-220.

[22] Niklasson, Bo. "Sindbis and Sindbis-like viruses." *The arboviruses*. CRC Press, 2019. 167-176.

[23] Das Sarma, J et al. “Mouse hepatitis virus type-2 infection in mice: an experimental model system of acute meningitis and hepatitis.” *Experimental and molecular pathology* vol. 71,1 (2001): 1-12. doi:10.1006/exmp.2001.2378

[24] Hernandez, Raquel, Christine Sinodis, and Dennis T. Brown. "Sindbis virus: propagation, quantification, and storage." *Current protocols in microbiology* 16.1 (2010): 15B-1.

[25] *XL10-Gold® Ultracompetent Cells transformation protocol* (no date) *Agilent*.Available at: https://www.agilent.com/en/product/mutagenesis-cloning/competent-cells-competent-cell-supplies/competent-cells-for-difficult-cloning/xl10-gold-ultracompetent-cells-233087 (Accessed: 07 November 2023).

[26] Ramsey, Jolene, et al. "Palmitoylation of Sindbis virus TF protein regulates its plasma membrane localization and subsequent incorporation into virions." *Journal of virology* 91.3 (2017): 10-1128.

[27] *Capped RNA synthesis (E2040)* (no date) *NEB*. Available at: https://www.neb.com/en-us/protocols/0001/01/01/capped-rna-synthesis-e2040 (Accessed: 08 November 2023).

[28] Navas, Sonia, et al. "Murine coronavirus spike protein determines the ability of the virus to replicate in the liver and cause hepatitis." *Journal of virology* 75.5 (2001): 2452-2457.

[29] Das Sarma, Jayasri, et al. "Enhanced green fluorescent protein expression may be used to monitor murine coronavirus spread in vitro and in the mouse central nervous system." *Journal of neurovirology* 8.5 (2002): 381-391.

APPENDIX A

PYTHON CODE

Using Python 3.9 all imported libraries are included at the top of every set of code, capable of running any computer that runs Python 3.9 and the required libraries.

This section includes the Python code for the alignment of the spike proteins of MHV and PENN98.

```
import jellyfish


A='MLFVFILFLPSCLGYIGDFRCIQLVNSNGANVSAPSISTETVEVSQGLGTYYVLDRVYLNATLLL
TGYYPVDGSKFRNLALTGTNSVSLSWFQPPYLSQFNDGIFAKVQNLKTSTPSGATAYFPTIVIGSL
FGYTSYTVVIEPYNGVIMASVCQYTICQLPYTDCKPNTNGNKLIGFWHTDVKPPICVLKRNFTLNV
NADAFYFHFYQHGGTFYAYYADKPSATTFLFSVYIGDILTQYYVLPFICNPTAGSTFAPRYWVTPL
VKRQYLFNFNQKGVITSAVDCASSYTSEIKCKTQSMLPSTGVYELSGYTVQPVGVVYRRVANLP
ACNIEEWLTARSVPSPLNWERKTFQNCNFNLSSLLRYVQAESLFCNNIDASKVYGRCFGSISVDK
FAVPRSRQVDLQLGNSGFLQTANYKIDTAATSCQLHYTLPKNNVTINNHNPSSWNRRYGFNDAG
VFGKNQHDVVYAQQCFTVRSSYCPCAQPDIVSPCTTQTKPKSAFVNVGDHCEGLGVLEDNCGN
ADPHKGCICANNSFIGWSHDTCLVNDRCQIFANILLNGINSGTTCSTDLQLPNTEVVTGICVKYDL
YGITGQGVFKEVKADYYNSWQTLLYDVNGNLNGFRDLTTNKTYTIRSCYSGRVSAAFHKDAPEP
ALLYRNINCSYVFSNNISREENPLNYFDSYLGCVVNADNRTDEALPNCDLRMGAGLCVDYSKSR
RAHRSVSTGYRLTTFEPYTPMLVNDSVQSVDGLYEMQIPTNFTIGHHEEFIQTRSPKVTIDCAAFV
CGDNTACRQQLVEYGSFCVNVNAILNEVNNLLDNMQLQVASALMQGVTISSRLPDGISGPIDDIN
FSPLLGCIGSTCAEDGNGPSAIRGRSAIEDLLFDKVKLSDVGFVEAYNNCTGGQEVRDLLCVQSF
NGIKVLPPVLSESQISGYTTGATAAAMFPPWSAAAGVPFSLSVQYRINGLGVTMNVLSENQKMIA
SAFNNALGAIQDGFDATNSALGKIQSVVNANAEALNNLLNQLSNRFGAISASLQEILTRLEAVEAK
AQIDRLINGRLTALNAYISKQLSDSTLIKVSAAQAIEKVNECVKSQTTRINFCGNGNHILSLVQNAP
YGLYFIHFSYVPISFTTANVSPGLCISGDRGLAPKAGYFVQDDGEWKFTGSSYYYPEPITDKNSVI
MSSCAVNYTKAPEVFLNTSIPNPPDFKEELDKWFKNQTSIAPDLSLDFEKLNVTLLDLTYEMNRIQ
DAIKKLNESYINLKEVGTYEMYVKWPWYVWLLIGLAGVAVCVLLFFICCCTGCGSCCFKKCGNCC
DEYGGHQDSIVIHNISSHED*'

B='MLFVFLTLLPSSLGYIGDFRCIQLVNTDTSNASAPSVSTEVVDVSKGIGTYYVLDRVYLNATLLL
TGYYPVDGSMYRNMALTGINTISLNWYKPPFLSEFNDGIFAKVKNLKASLPKDSISYFPTIIIGSNF
VTTSYTVVLEPYNGIIMASICQYTICQLPYTDCKPNTGGNKLIGFWHTELKSPVCILKRNFTFNVNA
EWLYFHFYQQGGTFYAYYADVSSATTFLFSMYIGDVLTQYFVLPYMCTLTTTGVFSPQYWVTPL
VKRQYLFNFNQKGIITSAVDCASSYTSEIKCKTQSMNPNTGVYDLSGYTVQPVGLVYRRVRNLPD
CKIEEWLTAKSVPSPLNWERKTFQNCNFDLSSLLRFVQAESLSCSNIDASKVYGMCFGSISIDKF
AIPNRRRVDLQLGNSGFLQSFNYKIDTRATSCQLYYSLAKNNVTVNNHNPSSWNRRYGFNDVAT
FGTGKHDVAYAEACFTVGASYCPCANPSIVSPCTTGKPNFANCPTGTSNRECTVMPLANNQFK
CDCTCNPSPLTTYDLRCLQARSMLGVGDHCEGLGVLEDKCGGSNTCNCSAHAFVGWAKDSCL
```

```
ANGRCHIFSNLMLNGINSGTTCSMDLQLPNTEVVTGVCVKYDLYGITGQGIFKEVKADYYHSWQ
NLLYDVNGNLIGFRDFVANKSYTIRSCYSGRVSAAYHQDAPEPALLYRNLKCDYVFNNNISREET
PLNYFDSYLGCVVNADNSTEEAVDACDLRMGSGLCVNYSTSHRARSSVSTGYKLTTFEPFTVRI
VNDSVESVDGLYELQIPTNFTIASHQEFVQTRSPKVTIDCAAFVCGGHTACRQQLVEYGSFCDNI
NAILGEVNNLIDTMQLQVASALIQGVTLSSRLSDGIGGQIDDINFSPLLGCLGSDCGEVTMAAQTG
RSAIEDVLFDKVKLSDVGFVEAYNNCTGGQEVRDLLCVQSFNGIKVLPPVLSENQISGYTAGATV
SAMFPWSAAAGVPFSLSVQYRINGLGVTMNVLSENQKMIASAFNNAIGAIQEGFAATNSALAKM
QFVVNANAEALNNLLNQLSNRFGAISASLQEILSRLDALEAQAQIDRLINGRLTALNAYVSKQLSD
MTLVKVSAAQAIEKVNECVKSQSSRINFCGNGNHILSLVQNAPYGLYFIHFSYVPTSFTTANVSPG
LCISGDRGLAPKAGYFVQDDGEWKFTGSNYYYPEPITDKNSVVMSSCAANYTKAPEVFLNTSIP
NLPDFKEELDKWFKNQTSIAPDLSLDFEKLNVTLLDLTDEMNRIQDAIKKLNESYINLKDVGTYEM
YVKWPWYVWLLIGLAGVAVCVLLFFICCCTGCGSCCFKKCGNCCDECGGHQDSIVIHNISSHED'

lenA=len(A)


D=jellyfish.levenshtein_distance(A, B)


Val=(D/lenA)


E=jellyfish.jaro_distance(A, B)


F=jellyfish.damerau_levenshtein_distance(A, B)


G=jellyfish.hamming_distance(A, B)


ValPer=(G/lenA)*100
```

This section includes the Python code for the scrapping of the Nanosight results pdf files for MHV and PENN98. Code modified from stack overflow.

```
## scraping data
```

```
import os                    # provides functions for creating and removing a directory (folder), fetching its contents, changing and identifying the current directory

import pandas as pd          # flexible open source data analysis/manipulation tool

import pdfplumber

import PyPDF2

import glob


#pdf = pdfplumber.open('-3 wt mhv 2022-01-05 15-48-56-ExperimentReport.pdf')


#page = pdf.pages[0] #so it only reads page one




# defining the functions used in main()

def get_keyword(start, end, text):
    """
    start: should be the word prior to the keyword.
    end: should be the word that comes after the keyword.
    text: represents the text from the page(s) you've just extracted.
    """
    for i in range(len(start)):
        try:
            field = ((text.split(start[i]))[1].split(end[i])[0])
            return field
        except:
            continue
```

```
def main():

    # create an empty dataframe, from which keywords from multiple .pdf files will be later
appended by rows.

    my_dataframe = pd.DataFrame()



    for files in glob.glob("pdfs/*.pdf"):

        with pdfplumber.open(files) as pdf:

            page = pdf.pages[0]

            text = page.extract_text()

            text = " ".join(text.split())

            text

            print(text)



            # use the function get_keyword as many times to get all the desired keywords from a pdf
document.



            # obtain keyword #1 : Mean

            start = ['Mean: ']

            end = [' nm']

            keyword1 = get_keyword(start, end, text)



            # obtain keyword #2 : Mode

            start = ['Mode: ']

            end = [' nm']

            keyword2 = get_keyword(start, end, text)
```

```
# obtain keyword #3 Standared deviation
start = ['SD: ']
end = [' nm']
keyword3 = get_keyword(start, end, text)

# obtain keyword #4 D10
start = ['D10: ']
end = [' nm']
keyword4 = get_keyword(start, end, text)

# obtain keyword #5 D50
start = ['D50: ']
end = [' nm']
keyword5 = get_keyword(start, end, text)

# obtain keyword #6 D90
start = ['D90: ']
end = [' nm']
keyword6 = get_keyword(start, end, text)

# obtain keyword #7 Mean
start = ['Mean: ']
end = [' nm Pre-treatment: ']
keyword7 = get_keyword(start, end, text)

# obtain keyword #8 Mean error
```

```
start = ['+/-']

end = ['nm Script Used:']

keyword8 = get_keyword(start, end, text)


# obtain keyword #9 mode

start = ['txt Mode: ']

end = ['+/-']

keyword9 = get_keyword(start, end, text)


# obtain keyword #10 mode error

start = ['+/-']

end = ['nm Time Captured:']

keyword10 = get_keyword(start, end, text)


# obtain keyword #11 SD

start = [' SD: ']

end = ['+/-']

keyword11 = get_keyword(start, end, text)


# obtain keyword #12 SD error

start = ['+/-']

end = ['nm Operator:']

keyword12 = get_keyword(start, end, text)


# obtain keyword #13 d10

start = ['D10:']

end = ['+/-']
```

```
keyword13 = get_keyword(start, end, text)

# obtain keyword #14 D10 error
start = ['+/-']
end = ['nm Pre-treatment:']
keyword14 = get_keyword(start, end, text)

# obtain keyword #15 D50
start = ['Pre-treatment: D50: ']
end = ['+/-']
keyword15 = get_keyword(start, end, text)

# obtain keyword #16 D50 error
start = ['+/-']
end = ['nm Sample Name:']
keyword16 = get_keyword(start, end, text)

# obtain keyword #17 D90
start = ['D90:']
end = ['+/-']
keyword17 = get_keyword(start, end, text)

# obtain keyword #18 Concentration
start = ['Concentration:']
end = ['+/-']
keyword18 = get_keyword(start, end, text)
```

```
        # obtain keyword #19 concentration error

        start = ['+/-']

        end = ['particles/ml Remarks:']

        keyword19 = get_keyword(start, end, text)


        # obtain keyword #20 particles/ frame

        start = ['particles/ml']

        end = ['+/-']

        keyword20 = get_keyword(start, end, text)




        # create a list with the keywords extracted from current document.

        my_list = [keyword1, keyword2, keyword3, keyword4, keyword5, keyword6, keyword7,
keyword8, keyword9, keyword10, keyword11, keyword12, keyword13, keyword14, keyword15,
keyword16, keyword17, keyword18, keyword19, keyword20 ]



        # append my list as a row in the dataframe.

        my_list = pd.Series(my_list)


        # append the list of keywords as a row to my dataframe.

        my_dataframe = my_dataframe.append(my_list, ignore_index=True)


        print("Document's keywords have been extracted successfully!")


    # rename dataframe columns using dictionaries.

    my_dataframe = my_dataframe.rename(columns={0:'Mean',

                                        1:'Mode',

                                        2:'SD',
```

```
                                    3:'D10',
                                    4:'D50',
                                    5:'D90',
                                    6:'Mean',
                                    7:'Mean error',
                                    8:'Mode',
                                    9:'Mode error',
                                    10:'SD',
                                    11:'SD error',
                                    12:'D10',
                                    13:'D10 error',
                                    14:'D50 ',
                                    15:'D50 error',
                                    16:'D90',
                                    17:'Concentration',
                                    18:'Concentration error',
                                    19:'Particles per frame'})

# change my current working directory
save_path = ('pdfs/')
os.chdir(save_path)

# extract my dataframe to an .xlsx file!
my_dataframe.to_excel('sample_excel.xlsx', sheet_name = 'my dataframe')
print("")
print(my_dataframe)
```

```
if __name__ == '__main__':
    main()
```